

Vector meson photoproduction with an effective Lagrangian in the quark model

Qiang Zhao and Zhenping Li

Department of Physics, Peking University, Beijing, 100871, People's Republic of China

C. Bennhold

Department of Physics, Center for Nuclear Studies, The George Washington University, Washington, D.C., 20052

(Received 18 November 1997)

A quark model approach to the photoproduction of vector mesons off nucleons is proposed. Its starting point is an effective Lagrangian of the interaction between the vector meson and the quarks inside the baryon, which generates the nondiffractive s- and u-channel resonance contributions. Additional t-channel π^0 and σ exchanges are included for the ω and ρ^0 production, respectively, to account for the large diffractive behavior in the small t region as suggested by Friman and Soyeur. The numerical results are presented for the ω and ρ productions in four isospin channels with the same set of parameters, and they are in good agreement with the available data not only in ω and ρ^0 productions, but also in the charged ρ productions where the additional t-channel σ exchange does not contribute so that it provides an important test to this approach. The investigation is also extended to the ϕ photoproduction, and the initial results show that the nondiffractive behavior of the ϕ productions in the large t region can be described by the s- and u-channel contributions with significantly smaller coupling constants, which is consistent with the findings in the similar studies in the QHD framework. The numerical investigation has also shown that polarization observables are essential for identifying so-called "missing resonances." [S0556-2813(98)07510-4]

PACS number(s): 13.75.Gx, 13.40.Hq, 13.60.Le

I. INTRODUCTION

The newly established electron and photon facilities have made it possible to investigate the mechanism of vector meson photoproductions on nucleons with much improved experimental accuracy. This has been motivated in part by the puzzle that the NRQM [1,2] predicts a much richer resonance spectrum than has been observed in $\pi N \rightarrow \pi N$ scattering experiments. Quark model studies have suggested that those resonances missing in the πN channel may couple strongly to, for example, the ωN and ρN channels. Experiments have been performed at ELSA [3] and will be done at TJNAF in the near future [4]. Therefore, a theory on the reaction mechanism that highlights the dynamical role of s-channel resonances is crucial in order to establish the "missing resonances" in the forthcoming experimental data for the vector meson, in particular ω and ρ , photoproductions.

The experimental and theoretical studies on vector meson photoproductions have a long history since the first experiment carried out on the Cambridge Electron Accelerator in 1964. There have been some experimental data of the vector meson photoproductions in their threshold regions where the s-channel resonances are expected to play an important role, for instance, the data from Ref. [3,5-7] for the ω and ρ photoproduction ($E_\gamma^{thres} \approx 1.11$ GeV), and the data from Ref. [8] for the ϕ photoproduction ($E_\gamma^{thres} \approx 1.57$ GeV). Historically, these studies have concentrated on the diffractive behavior in the small t region for the neutral meson (ω , ρ^0 , and ϕ) productions, in which it has been shown that the vector meson dominance model (VMD) [9] gives a good description in the low energy region, while the Pomeron exchange becomes more important as the energy increases [10]. The focus of this paper is not on the large diffractive behavior in the small t region, but rather on the nondiffractive s- and

u-channel contributions in the large t region in which the t-channel Pomeron exchange becomes less significant. Furthermore, we will attempt to provide a unified framework for both neutral and charged vector meson productions. Since the t-channel exchanges responsible for the large diffractive behavior in the small t region, such as the Pomeron exchange, do not contribute to the charged meson productions, the nondiffractive s- and u-channel resonances become more dominant, thus, they provide a crucial test to any model that concentrates on the role of the s- and u-channel resonances in the vector meson photoproductions. The quark model approach provides an ideal framework to investigate the dynamical role of the s- and u-channel resonances in the vector meson photoproductions. The studies in the pseudoscalar photoproductions have shown [11] that every s- and u-channel resonance, particularly, those high partial wave resonances such as F_{15} and F_{37} , can be taken into account, and this has been proven to be very difficult for the traditional approach at the hadronic level. Moreover, it introduces the quark degrees of freedom directly into the reaction mechanism, thus gives a very good description to the pseudoscalar meson productions with much less parameters than the models at the hadronic level. It is therefore natural to extend this approach to the vector meson photoproductions in the resonance region.

A major difference for the vector meson production from the pseudoscalar meson case in the quark model is that the interaction between the vector mesons and the quarks inside the baryon is largely unknown. Although phenomenological models have been developed to evaluate baryon resonance decaying into a nucleon and a vector meson, such as the quark pair creation model [12] or the 3P_0 model, these approaches are unsuitable for the description of vector meson

photoproductions. This is due to the fact that they only yield transition amplitudes for s-channel resonances, but contain no information on how to derive the nonresonant terms in the u- and t-channels. Therefore, we choose an effective Lagrangian here as our starting point that satisfies the fundamental symmetries and determines the transition amplitudes not only in the s-channel, but also in the u- and t-channels.

Even though the effective Lagrangians are different from each other for pseudoscalar and vector meson photoproductions, the implementation follows the same guidelines. The transition amplitudes for each resonance in the s-channel below 2 GeV will be included explicitly, while the resonances above 2 GeV for a given quantum number n in the harmonic oscillator basis of the quark model are treated as degenerate, so that their transition amplitudes can be written in a compact form. Similarly, the excited resonances in the u-channel are assumed to be degenerate as well. Only the mass splitting between the spin 1/2 and spin 3/2 resonances with $n=0$ in the harmonic oscillator basis, such as the splitting between nucleon and Δ resonance, is found to be significant, thus, the transition amplitudes for the spin 3/2 resonance with $n=0$ in the u-channel will be included separately.

The effective Lagrangian employed here generates not only the s- and u-channel exchanges, but also a t-channel term containing the vector meson exchange. For charged vector mesons gauge invariance also mandates a seagull term. Although in principle, all the contributions from resonances have been included in the effective Lagrangian, we do not expect that such an approach can give an agreement with the data in the small t region in the neutral vector meson photoproductions since additional t-channel contribution, such as the Pomeron exchange, will be responsible for the strong diffractive behavior in the small t region. As it has been shown in Ref. [13] and also in Ref. [14] and Ref. [15] about the diffraction duality, there can be a nonresonant imaginary background amplitude in neutral vector meson, such as ω and ρ^0 photoproductions, but not in the charged vector meson ρ^\pm photoproductions. Therefore, the large difference of the cross section between the neutral and charged ρ meson photoproduction, observed in the direct channel resonance region, is due to such a background amplitude, and it should be from the large contribution of the Pomeron singularity in the neutral photoproduction from high energies down to the threshold. This has been one of our concerns in the numerical investigations. Therefore, we add a t-channel π^0 exchange to the amplitude for ω photoproduction and a σ exchange term to the amplitude for ρ^0 photoproduction suggested by Friman and Soyeur [16] who showed these two terms play dominant roles in ω and ρ^0 productions, respectively, over other meson exchange processes near the threshold.

With the above considerations, we apply our model to the five isospin channels, $\gamma p \rightarrow \omega p$, $\gamma p \rightarrow \rho^0 p$, $\gamma n \rightarrow \rho^- p$, $\gamma p \rightarrow \rho^+ n$ and $\gamma p \rightarrow \phi p$. With the same set of parameters introduced in our model, we obtained an overall agreement with the differential cross sections in the large t region for the first four channels, while with relatively smaller parameters in the ϕ photoproduction, we predict the behavior of the differential cross section in the large t region. With the additional t-channel π^0 and σ exchanges included in the ω and ρ^0 photoproduction, respectively, we obtain an overall agree-

ment with the available data from small t to large t region. The overall agreement between the theoretical predictions and the data available not only for the neutral meson ω and ρ^0 , but also for the charged meson ρ^\pm productions in which the s- and u-channel contributions become more dominant is remarkable. It is even more remarkable that both ω and ρ productions can be described by the same set of parameters, which is by no means trivial. It suggests that the quark model approach provides a very good framework to investigate the resonance structure in the vector meson photoproductions. Our results also show that polarization observables are crucial in determining the resonance structure, which has been shown to be the case in the pseudoscalar meson photoproductions.

In the reaction $\gamma p \rightarrow \phi p$. Since the threshold energy of the ϕ production is above the resonance region, the primary focus here is the ϕNN coupling constant. Because the production of $s\bar{s}$ from the nucleons should be suppressed under the Okubo-Zweig-Iizuka (OZI) rule, the ϕNN coupling constant is expected to be smaller than the ωNN or ρNN couplings. The recent experiment on the $p\bar{p} \rightarrow \phi X$ ($X = \pi, \eta, \omega, \rho, \pi\pi, \gamma$) [17] has shown a significant violation of the OZI rule, and it can not be explained by the diffractive process, such as Pomeron exchange. Thus, large contributions from the nondiffractive processes are expected to contribute to the ϕ photoproduction near the threshold. This has been the subject of many studies, such as the recently developed quantum hadrodynamical (QHD) model approach [18]. In our framework, it could be achieved by fitting the s- and u-channel contributions to the differential cross sections of ϕ productions in the large t region [8], where the contributions from the Pomeron exchange become less significant. The initial results show that the ϕNN couplings in the quark model are small, but significant which is consistent with those in the QHD approach.

In Sec. II, we briefly discuss some of the observables used in our approach, which have been developed extensively in Ref. [19]. The framework for the vector meson photoproductions with effective Lagrangian for the quark-meson interaction is presented in Sec. III. In Sec. IV, we show our numerical studies of the ω , ρ , and ϕ photoproductions in the five isospin channels. Finally, conclusions will be presented in Sec. V.

II. OBSERVABLES AND HELICITY AMPLITUDES

Before presenting our quark model approach, we introduce some general features of vector meson photoproduction on the nucleon. The basic amplitude \mathcal{F} for $\gamma + N \rightarrow V + N'$ is defined as

$$\mathcal{F} = \langle \mathbf{q} \lambda_V \lambda_2 | T | \mathbf{k} \lambda \lambda_1 \rangle, \quad (1)$$

where \mathbf{k} and \mathbf{q} are the momenta of the incoming photon and outgoing vector meson. The helicity states are denoted by $\lambda = \pm 1$ for the incident photon, $\lambda_V = 0, \pm 1$ for the outgoing vector meson, and $\lambda_1 = \pm 1/2$, $\lambda_2 = \pm 1/2$ for the initial and final state nucleons, respectively. Following Ref. [19], the amplitude \mathcal{F} can be expressed as a 6×4 matrix in the helicity space,

$$\mathcal{F} = \begin{pmatrix} H_{21} & H_{11} & H_{3-1} & -H_{4-1} \\ H_{41} & H_{31} & -H_{1-1} & H_{2-1} \\ H_{20} & H_{10} & -H_{30} & H_{40} \\ H_{40} & H_{30} & H_{10} & -H_{20} \\ H_{2-1} & H_{1-1} & H_{31} & -H_{41} \\ H_{4-1} & H_{3-1} & -H_{11} & H_{21} \end{pmatrix}. \quad (2)$$

Because of the parity conservation,

$$\langle \mathbf{q} \lambda_V \lambda_2 | T | \mathbf{k} \lambda \lambda_1 \rangle = (-1)^{\Lambda_f - \Lambda_i} \langle \mathbf{q} -\lambda_V -\lambda_2 | T | \mathbf{k} -\lambda -\lambda_1 \rangle, \quad (3)$$

where $\Lambda_f = \lambda - \lambda_1$ and $\Lambda_i = \lambda_V - \lambda_2$ in the Jacob-Wick (JW) convention, the $H_{a\lambda_V}(\theta)$ in Eq. (2) reduces to 12 independent complex helicity amplitudes:

$$\begin{aligned} H_{1\lambda_V} &= \langle \lambda_V, \lambda_2 = +1/2 | T | \lambda = 1, \lambda_1 = -1/2 \rangle \\ H_{2\lambda_V} &= \langle \lambda_V, \lambda_2 = +1/2 | T | \lambda = 1, \lambda_1 = +1/2 \rangle \\ H_{3\lambda_V} &= \langle \lambda_V, \lambda_2 = -1/2 | T | \lambda = 1, \lambda_1 = -1/2 \rangle \\ H_{4\lambda_V} &= \langle \lambda_V, \lambda_2 = -1/2 | T | \lambda = 1, \lambda_1 = +1/2 \rangle. \end{aligned} \quad (4)$$

Each experimental observable Ω can be written in the general *bilinear helicity product* (BHP) form,

$$\begin{aligned} \check{\Omega}^{\alpha\beta} &= \Omega^{\alpha\beta} \mathcal{T}(\theta) \\ &= \pm \frac{1}{2} \langle H | \Gamma^\alpha \omega^\beta | H \rangle \\ &= \pm \frac{1}{2} \sum_{a,b,\lambda_V,\lambda_V'} H_{a\lambda_V}^* \Gamma_{ab}^\alpha \omega_{\lambda_V\lambda_V'}^\beta H_{b\lambda_V'}. \end{aligned} \quad (5)$$

For example, the differential cross section operator is given by

$$\begin{aligned} \check{\Omega}^{\alpha=1,\beta=1} &= \mathcal{T}(\theta) \\ &= \frac{1}{2} \langle H | \boxed{\Gamma^1} \boxed{\omega^1} | H \rangle \\ &= \frac{1}{2} \sum_{a=1}^4 \sum_{\lambda_V=0,\pm 1} |H_{a\lambda_V}|^2, \end{aligned} \quad (6)$$

where the box frames denote the diagonal structure of the matrices. The Γ and ω matrices labeled by different α and β correspond to different spin observables. With the phase space factor, the differential cross section has the expression

$$\begin{aligned} \frac{d\sigma}{d\Omega_{c.m.}} &= (\text{p.s. factor}) \mathcal{T}(\theta) \\ &= \frac{\alpha_e \omega_m (E_f + M_N)(E_i + M_N)}{8\pi s} \\ &\quad \times |\mathbf{q}| \frac{1}{2} \sum_{a=1}^4 \sum_{\lambda_V=0,\pm 1} |H_{a\lambda_V}|^2 \end{aligned} \quad (7)$$

in the center of mass frame, where \sqrt{s} is the total energy of the system, E_i and E_f are the energies of the nucleons in the initial and final states, respectively. M_N represents the masses of the nucleon and ω_m denotes the energy of the outgoing meson.

These helicity amplitudes are usually related to the density matrix elements ρ_{ik} [20], which are measured by the experiments [21]. They are defined as

$$\begin{aligned} \rho_{ik}^0 &= \frac{1}{A} \sum_{\lambda\lambda_2\lambda_1} H_{\lambda_V\lambda_2,\lambda\lambda_1} H_{\lambda_V\lambda_2,\lambda\lambda_1}^*, \\ \rho_{ik}^1 &= \frac{1}{A} \sum_{\lambda\lambda_2\lambda_1} H_{\lambda_V\lambda_2,-\lambda\lambda_1} H_{\lambda_V\lambda_2,\lambda\lambda_1}^*, \\ \rho_{ik}^2 &= \frac{i}{A} \sum_{\lambda\lambda_2\lambda_1} \lambda H_{\lambda_V\lambda_2,-\lambda\lambda_1} H_{\lambda_V\lambda_2,\lambda\lambda_1}^*, \\ \rho_{ik}^3 &= \frac{i}{A} \sum_{\lambda\lambda_2\lambda_1} \lambda H_{\lambda_V\lambda_2,\lambda\lambda_1} H_{\lambda_V\lambda_2,\lambda\lambda_1}^*, \end{aligned} \quad (8)$$

where

$$A = \sum_{\lambda_V\lambda\lambda_2\lambda_1} H_{\lambda_V\lambda_2,\lambda\lambda_1} H_{\lambda_V\lambda_2,\lambda\lambda_1}^*, \quad (9)$$

where ρ_{ik} stands for $\rho_{\lambda_V\lambda_2,\lambda\lambda_1}$, and $\lambda_{V_i}, \lambda_{V_k}$ denote the helicity of the produced vector mesons.

For example, the angular distribution for ρ^0 decaying into $\pi^+\pi^-$ produced by linearly polarized photons can be expressed in terms of nine independent measurable spin-density matrix elements

$$\begin{aligned} W(\cos \theta, \phi, \Phi) &= \frac{3}{4\pi} \left[\frac{1}{2} (1 - \rho_{00}^0) + \frac{1}{2} (3\rho_{00}^0 - 1) \cos^2 \theta \right. \\ &\quad - \sqrt{2} \text{Re } \rho_{10}^0 \sin 2\theta \cos \phi \\ &\quad - \rho_{1-1}^0 \sin^2 \theta \cos 2\phi - P_\gamma \cos 2\Phi (\rho_{11}^1 \sin^2 \theta \\ &\quad + \rho_{00}^1 \cos^2 \theta - \sqrt{2} \text{Re } \rho_{10}^1 \sin 2\theta \cos \phi \\ &\quad - \rho_{1-1}^1 \sin^2 \theta \cos 2\phi) \\ &\quad - P_\gamma \sin 2\Phi (\sqrt{2} \text{Im } \rho_{10}^2 \sin 2\theta \sin \phi \\ &\quad \left. + \text{Im } \rho_{1-1}^2 \sin^2 \theta \sin 2\phi) \right], \end{aligned} \quad (10)$$

where P_γ is the degree of the linear polarization of the photon, Φ is the angle of the photon electric polarization vector with respect to the production plane measured in the c.m. system, and θ and ϕ are the polar and azimuthal angles of the π^+ which is produced by the ρ^0 decay in the ρ^0 rest frame.

III. QUARK MODEL APPROACH FOR VECTOR MESON PHOTOPRODUCTION

The starting point of the quark model approach is the effective Lagrangian,

$$L_{\text{eff}} = -\bar{\psi}\gamma_{\mu}p^{\mu}\psi + \bar{\psi}\gamma_{\mu}e_q A^{\mu}\psi + \bar{\psi}\left(a\gamma_{\mu} + \frac{ib\sigma_{\mu\nu}q^{\nu}}{2m_q}\right)\phi_m^{\mu}\psi, \quad (11)$$

where the quark field ψ is expressed as

$$\psi = \begin{pmatrix} \psi(u) \\ \psi(d) \\ \psi(s) \end{pmatrix}, \quad (12)$$

and the meson field ϕ_m^{μ} is a $3 \otimes 3$ matrix,

$$\phi_m = \begin{pmatrix} \frac{1}{\sqrt{2}}\rho^0 + \frac{1}{\sqrt{2}}\omega & \rho^+ & K^{*+} \\ \rho^- & -\frac{1}{\sqrt{2}}\rho^0 + \frac{1}{\sqrt{2}}\omega & K^{*0} \\ K^{*-} & \bar{K}^{*0} & \phi \end{pmatrix} \quad (13)$$

in which the vector mesons are treated as pointlike particles. At tree level, the transition matrix element based on the effective Lagrangian in Eq. (11) can be written as the sum of contributions from the s-, u-, and t-channels,

$$M_{fi} = M_{fi}^s + M_{fi}^u + M_{fi}^t, \quad (14)$$

where the s- and u-channel contributions in Eq. (14) have the following form:

$$M_{fi}^s + M_{fi}^u = \sum_j \langle N_f | H_m | N_j \rangle \langle N_j | \frac{1}{E_i + \omega - E_j} H_e | N_i \rangle + \sum_j \langle N_f | H_e \frac{1}{E_i - \omega_m - E_j} | N_j \rangle \langle N_j | H_m | N_i \rangle, \quad (15)$$

where the electromagnetic coupling vertex is

$$H_e = -\bar{\psi}\gamma_{\mu}e_q A^{\mu}\psi, \quad (16)$$

and the quark-meson coupling vertex is

$$H_m = -\bar{\psi}\left(a\gamma_{\mu} + \frac{ib\sigma_{\mu\nu}q^{\nu}}{2m_q}\right)\phi_m^{\mu}\psi, \quad (17)$$

where m_q is the quark mass and the constants a and b in Eqs. (11) and (17) are the vector and tensor coupling constants, which will be treated as free parameters in our approach. The initial and final states of the nucleon are denoted by $|N_i\rangle$ and $|N_f\rangle$, respectively, and $|N_j\rangle$ is the intermediate resonance state, while E_i and E_j are the energies of the initial nucleon and the intermediate resonance.

An important test of the transition matrix elements

$$M_{fi} = \langle \lambda_2 | J_{\mu\nu} \epsilon^{\mu} \epsilon^{\nu} | \lambda_1 \rangle, \quad (18)$$

would be gauge invariance:

$$\langle \lambda_2 | J_{\mu\nu} k^{\mu} | \lambda_1 \rangle = \langle \lambda_2 | J_{\mu\nu} q^{\nu} | \lambda_1 \rangle = 0, \quad (19)$$

where ϵ_m^{μ} , ϵ^{ν} are the polarization vectors of the vector mesons and photons. However, we find that the condition $\langle \lambda_2 | J_{\mu\nu} q^{\nu} | \lambda_1 \rangle = 0$ is not satisfied for the t-channel vector meson exchange term,

$$M_{fi}^t = -a \langle N_f | \sum_l \frac{e_m}{2q \cdot k} \{ 2q \cdot \epsilon \gamma \cdot \epsilon_m - \gamma \cdot q \epsilon \cdot \epsilon_m + k \cdot \epsilon_m \gamma \cdot \epsilon \} e^{i(\mathbf{k}-\mathbf{q}) \cdot \mathbf{r}_l} | N_i \rangle, \quad (20)$$

based on the Feynman rules for the photon-vector meson coupling, and the relation

$$\langle N_f | \gamma \cdot (q-k) e^{i(\mathbf{k}-\mathbf{q}) \cdot \mathbf{r}_l} | N_i \rangle = 0. \quad (21)$$

To remedy this problem, we add a gauge fixing term, so that

$$M_{fi}^t = -a \langle N_f | \sum_l \frac{e_m}{2q \cdot k} 2 \{ q \cdot \epsilon \gamma \cdot \epsilon_m - \gamma \cdot q \epsilon \cdot \epsilon_m + k \cdot \epsilon_m \gamma \cdot \epsilon \} e^{i(\mathbf{k}-\mathbf{q}) \cdot \mathbf{r}_l} | N_i \rangle. \quad (22)$$

The techniques of deriving the transition amplitudes have been developed for Compton scattering [22]. Following the same procedure as given in Eq. (14) of Ref. [11], we can divide the photon interaction into two parts and the contributions from the s- and u-channel can be rewritten as

$$M_{fi}^{s+u} = i \langle N_f | [g_e, H_m] | N_i \rangle + i\omega \sum_j \langle N_f | H_m | N_j \rangle \langle N_j | \frac{1}{E_i + \omega - E_j} h_e | N_i \rangle + i\omega \sum_j \langle N_f | h_e \frac{1}{E_i - \omega_m - E_j} | N_j \rangle \langle N_j | H_m | N_i \rangle, \quad (23)$$

where

$$g_e = \sum_l e_l \mathbf{r}_l \cdot \boldsymbol{\epsilon} e^{i\mathbf{k} \cdot \mathbf{r}_l}, \quad (24)$$

$$h_e = \sum_l e_l \mathbf{r}_l \cdot \boldsymbol{\epsilon} (1 - \boldsymbol{\alpha} \cdot \hat{\mathbf{k}}) e^{i\mathbf{k} \cdot \mathbf{r}_l} \quad (25)$$

$$\hat{\mathbf{k}} = \frac{\mathbf{k}}{w}. \quad (26)$$

The first term in Eq. (23) can be identified as a seagull term; it is proportional to the charge of the outgoing vector meson. The second and third term in Eq. (23) represents the s- and u-channel contributions. Adopting the same strategy as in the pseudoscalar case, we include a complete set of helicity amplitudes for each of the s-channel resonances below 2 GeV in the $SU(6) \otimes O(3)$ symmetry limit. The resonances above 2 GeV are treated as degenerate in order to express each contribution from all resonances with quantum number n in a compact form. The contributions from the resonances with the largest spin for a given quantum number n were found to be the most important as the energy increases [11]. This corresponds to spin $J = n + 1/2$ with I

=1/2 for the reactions $\gamma N \rightarrow K^* \Lambda$ and $\gamma N \rightarrow \omega N$, and $J = n + 3/2$ with $I = 3/2$ for the reactions $\gamma N \rightarrow K^* \Sigma$ and $\gamma N \rightarrow \rho N$.

Similar to the pseudoscalar case, the contributions from the u-channel resonances are divided into two parts as well. The first part contains the resonances with the quantum number $n = 0$, which includes the spin 1/2 states, such as the Λ , Σ and the nucleons, and the spin 3/2 resonances, such as the Σ^* in K^* photoproduction and $\Delta(1232)$ resonance in ρ photoproduction. Because the mass splitting between the spin 1/2 and spin 3/2 resonances for $n = 0$ is significant, they have to be treated separately. The transition amplitudes for these u-channel resonances will also be written in terms of the helicity amplitudes. The second part comes from the excited resonances with quantum number $n \geq 1$. As the contributions from the u-channel resonances are not sensitive to the precise mass positions, they can be treated as degenerate as well, so that the contributions from these resonances can again be written in a compact form.

A. The Seagull term

The transition amplitude is divided into the transverse and longitudinal amplitudes according to the polarization of the outgoing vector mesons. The longitudinal polarization vector for a vector meson with mass μ and momentum \mathbf{q} is

$$\epsilon_L^\mu = \frac{1}{\mu} \begin{pmatrix} |\mathbf{q}| \\ \omega_m \mathbf{q} \\ |\mathbf{q}| \end{pmatrix}, \quad (27)$$

where $\omega_m = \sqrt{\mathbf{q}^2 + \mu^2}$ is the energy of the outgoing vector mesons. Thus, the longitudinal interaction at the quark-meson vertex can be written as

$$H_m^L = \epsilon_L^\mu J_\mu = \epsilon_0 J_0 - \epsilon_3 J_3 \quad (28)$$

where ϵ_3 corresponds to the direction of the momentum \mathbf{q} . The transition amplitudes of the s- and u-channel for the longitudinal quark-meson coupling become

$$\begin{aligned} M_{fi}^{s+u}(L) &= i \langle N_f | [g_e, H_m^L] | N_i \rangle - i \omega \langle N_f | \left[h_e, \frac{\epsilon_3}{q_3} J_0 \right] | N_i \rangle \\ &+ i \omega \sum_j \langle N_f | \left(\epsilon_0 - \frac{\omega_m}{q_3} \epsilon_3 \right) J_0 | N_j \rangle \\ &\times \langle N_j | \frac{1}{E_i + \omega - E_j} h_e | N_i \rangle \\ &+ i \omega \sum_j \langle N_f | h_e \frac{1}{E_i - \omega_m - E_j} | N_j \rangle \langle N_j | \\ &\times \left(\epsilon_0 - \frac{\omega_m}{q_3} \epsilon_3 \right) J_0 | N_i \rangle, \end{aligned} \quad (29)$$

where the first two terms are seagull terms which can be rewritten as,

$$\begin{aligned} M_{fi}^{Seagull}(L) &= - \frac{a \omega_m e_m}{\mu |\mathbf{q}|} \langle N_f | \boldsymbol{\alpha} \cdot \boldsymbol{\epsilon} e^{i(\mathbf{k}-\mathbf{q}) \cdot \mathbf{r}_l} | N_i \rangle \\ &- \frac{ia \mu e_m}{|\mathbf{q}|} \langle N_f | \sum_l \mathbf{r}_l \cdot \boldsymbol{\epsilon} e^{i(\mathbf{k}-\mathbf{q}) \cdot \mathbf{r}_l} | N_i \rangle. \end{aligned} \quad (30)$$

The first term will be cancelled by a corresponding term from the t-channel to keep the gauge invariance, while the second term has more explicit expression as

$$M_{fi}^{Seagull}(L) = - \frac{a \mu e_m}{|\mathbf{q}| \alpha^2} g_v^t \mathbf{q} \cdot \boldsymbol{\epsilon} e^{i(\mathbf{k}-\mathbf{q}) \cdot \mathbf{r}_l}, \quad (31)$$

where the g_v^t is defined as the following:

$$g_v^t = \langle N_f | \sum_j \hat{I}_j | N_i \rangle. \quad (32)$$

The values of g_v^t for every channel is presented in Table I. The corresponding expressions for the t-channel amplitudes are given in the Appendix. The last two terms in Eq. (29) will be discussed in the following sections.

The nonrelativistic expansion of the transverse meson quark interaction vertex gives

$$H_m^T = \sum_l \left\{ i \frac{b'}{2m_q} \boldsymbol{\sigma}_l \cdot (\mathbf{q} \times \boldsymbol{\epsilon}_v) + a \mathbf{A} \cdot \boldsymbol{\epsilon}_v + \frac{a}{2\mu_q} \mathbf{p}'_l \cdot \boldsymbol{\epsilon}_v \right\} \hat{I}_l e^{-i\mathbf{q} \cdot \mathbf{r}_l} \quad (33)$$

where $b' \equiv b - a$, \mathbf{p}'_l is the internal motion of the l th quark in the c.m. system, and

$$\hat{I}_l = \begin{cases} a_l^\dagger(s) a_l(u) & \text{for } K^{*+} \\ a_l^\dagger(s) a_l(d) & \text{for } K^{*0} \\ a_l^\dagger(d) a_l(u) & \text{for } \rho^+ \\ -\frac{1}{\sqrt{2}} (a_l^\dagger(u) a_l(u) - a_l^\dagger(d) a_l(d)) & \text{for } \rho^0 \\ 1 & \text{for } \omega(\phi). \end{cases} \quad (34)$$

The vector \mathbf{A} has the general form,

$$\mathbf{A} = \frac{\mathbf{P}_f}{E_f + M_f} + \frac{\mathbf{P}_i}{E_i + M_i}, \quad (35)$$

which comes from the center-mass motion of the quark system. In the s- and u-channel, \mathbf{A} has the following expression for different channels,

$$s\text{-channel: } \mathbf{A} = -\frac{\mathbf{q}}{E_f + M_f}, \quad (36)$$

$$u\text{-channel: } \mathbf{A} = -\left(\frac{1}{E_f + M_f} + \frac{1}{E_i + M_i}\right)\mathbf{k} - \frac{1}{E_f + M_f}\mathbf{q}. \quad (37)$$

The transverse transition amplitude for the s- and u-channel is

$$\begin{aligned} M_{fi}^{s+u}(T) &= i\langle N_f | [g_e, H_m^T] | N_i \rangle \\ &+ i\omega \sum_j \langle N_f | H_m^T | N_j \rangle \langle N_j | \frac{1}{E_i + \omega - E_j} h_e | N_i \rangle \\ &+ i\omega \sum_j \langle N_f | h_e \frac{1}{E_i - \omega_m - E_j} | N_j \rangle \langle N_j | H_m^T | N_i \rangle. \end{aligned} \quad (38)$$

The nonrelativistic expansion of the first term gives

$$\begin{aligned} M_{fi}^{Seagull}(T) &= -i\langle N_f | [g_e, H_m^T] | N_i \rangle \\ &= -ia e_m g_v^t \langle N_f | \left\{ \frac{\mathbf{P} \cdot \boldsymbol{\epsilon}_v}{E + M}, \mathbf{R} \cdot \boldsymbol{\epsilon} \right\} \\ &\quad \times e^{-(\mathbf{k}-\mathbf{q})^2/6\alpha^2} | N_i \rangle \\ &+ a e_m g_A \langle N_f | \left[\frac{\boldsymbol{\sigma} \cdot (\mathbf{P} \times \boldsymbol{\epsilon}_v)}{E + M}, \mathbf{R} \cdot \boldsymbol{\epsilon} \right] \\ &\quad \times e^{-(\mathbf{k}-\mathbf{q})^2/6\alpha^2} | N_i \rangle, \end{aligned} \quad (39)$$

where $\{A, B\} = AB + BA$ is the anticommutation operator. \mathbf{P} and \mathbf{R} are the momentum and coordinate of the center of mass motion of the three quark system.

The seagull terms in the transitions are proportional to the charge of the outgoing mesons and, therefore, vanish in the neutral vector meson, ω , ρ^0 , and ϕ , photoproductions.

B. U-channel transition amplitudes

The last term in Eq. (29) is the longitudinal transition amplitude in the u-channel. We find

$$\begin{aligned} M_{fi}^u(L) &= i\omega \sum_j \langle N_f | h_e \frac{1}{E_i - \omega_m - E_j} | N_j \rangle \langle N_j | -\frac{\mu}{|\mathbf{q}|} J_0 | N_i \rangle \\ &= (M_3^u + M_2^u) e^{-(\mathbf{q}^2 + \mathbf{k}^2)/6\alpha^2} \end{aligned} \quad (40)$$

in the harmonic oscillator basis, where

$$\begin{aligned} M_3^u &= g_3^u \frac{a\mu}{|\mathbf{q}|} \left[\frac{i}{2m_q} \boldsymbol{\sigma} \cdot (\boldsymbol{\epsilon} \times \mathbf{k}) F^0 \left(\frac{\mathbf{k} \cdot \mathbf{q}}{3\alpha^2}, P_f \cdot k \right) \right. \\ &\quad \left. - g_v \frac{\omega}{3\alpha^2} \mathbf{q} \cdot \boldsymbol{\epsilon} F^1 \left(\frac{\mathbf{k} \cdot \mathbf{q}}{3\alpha^2}, P_f \cdot k \right) \right], \end{aligned} \quad (41)$$

which corresponds to incoming photons and outgoing vector mesons being absorbed and emitted by the same quark, and

$$\begin{aligned} M_2^u &= g_2^u \frac{a\mu}{|\mathbf{q}|} \left[g'_a \frac{i}{2m_q} \boldsymbol{\sigma} \cdot (\boldsymbol{\epsilon} \times \mathbf{k}) F^0 \left(-\frac{\mathbf{k} \cdot \mathbf{q}}{6\alpha^2}, P_f \cdot k \right) \right. \\ &\quad \left. + g'_v \frac{\omega}{6\alpha^2} \mathbf{q} \cdot \boldsymbol{\epsilon} F^1 \left(-\frac{\mathbf{k} \cdot \mathbf{q}}{6\alpha^2}, P_f \cdot k \right) \right] \end{aligned} \quad (42)$$

in which the incoming photons and outgoing vector mesons are absorbed and emitted by different quarks. P_f in Eq. (41) and Eq. (42) denotes the four momentum of the final state nucleon. The function F in Eq. (41) and Eq. (42) is defined as

$$F^l(x, y) = \sum_{n \geq l} \frac{M_n}{(n-l)!(y+n\delta M^2)} x^{n-l}, \quad (43)$$

where $n\delta M^2 = (M_n^2 - M_f^2)/2$ represents the average mass difference between the ground state and excited states with the total excitation quantum number n in the harmonic oscillator basis. The parameter α^2 in the above equation is commonly used in the quark model and is related to the harmonic oscillator strength.

Similarly, the transverse transition in the u-channel is given by

$$\begin{aligned} M_{fi}^u(T) &= i\omega \sum_j \langle N_f | h_e \frac{1}{E_i - \omega_m - E_j} | N_j \rangle \langle N_j | H_m^T | N_i \rangle \\ &= (M_3^u + M_2^u) e^{-(\mathbf{q}^2 + \mathbf{k}^2)/6\alpha^2}, \end{aligned} \quad (44)$$

where

$$\begin{aligned} M_3^u/g_3^u &= \frac{b'}{4m_q^2} \{g_v (\boldsymbol{\epsilon} \times \mathbf{k}) \cdot (\mathbf{q} \times \boldsymbol{\epsilon}_v) + i\boldsymbol{\sigma} \cdot (\boldsymbol{\epsilon} \times \mathbf{k}) \times (\mathbf{q} \times \boldsymbol{\epsilon}_v)\} F^0 \left(\frac{\mathbf{k} \cdot \mathbf{q}}{3\alpha^2}, P_f \cdot k \right) - \frac{ia}{2m_q} \boldsymbol{\sigma} \cdot (\boldsymbol{\epsilon} \times \mathbf{k}) \mathbf{A} \cdot \boldsymbol{\epsilon}_v F^0 \left(\frac{\mathbf{k} \cdot \mathbf{q}}{3\alpha^2}, P_f \cdot k \right) \\ &+ \left(\frac{ia}{12m_q^2} \boldsymbol{\sigma} \cdot (\boldsymbol{\epsilon} \times \mathbf{k}) \boldsymbol{\epsilon}_v \cdot \mathbf{k} + \frac{ib'\omega}{6m_q\alpha^2} \boldsymbol{\sigma} \cdot (\mathbf{q} \times \boldsymbol{\epsilon}_v) \boldsymbol{\epsilon} \cdot \mathbf{q} + g_v \frac{a\omega}{3\alpha^2} \boldsymbol{\epsilon} \cdot \mathbf{q} \mathbf{A} \cdot \boldsymbol{\epsilon}_v - g_v \frac{a\omega}{6m_q} \boldsymbol{\epsilon} \cdot \boldsymbol{\epsilon}_v \right) F^1 \left(\frac{\mathbf{k} \cdot \mathbf{q}}{3\alpha^2}, P_f \cdot k \right) \\ &- g_v \frac{a\omega}{18m_q\alpha^2} \boldsymbol{\epsilon}_v \cdot \mathbf{k} \boldsymbol{\epsilon} \cdot \mathbf{q} F^2 \left(\frac{\mathbf{k} \cdot \mathbf{q}}{3\alpha^2}, P_f \cdot k \right) \end{aligned} \quad (45)$$

and

$$\begin{aligned}
 M_2^u/g_2^u &= \frac{b'}{4m_q^2} \{g'_v(\boldsymbol{\epsilon} \times \mathbf{k}) \cdot (\mathbf{q} \times \boldsymbol{\epsilon}_v) - ig'_a \boldsymbol{\sigma} \cdot (\boldsymbol{\epsilon} \times \mathbf{k}) \times (\mathbf{q} \times \boldsymbol{\epsilon}_v)\} F^0\left(-\frac{\mathbf{k} \cdot \mathbf{q}}{6\alpha^2}, P_f \cdot k\right) - \frac{ia}{2m_q} \boldsymbol{\sigma} \cdot (\boldsymbol{\epsilon} \times \mathbf{k}) \mathbf{A} \cdot \boldsymbol{\epsilon}_v F^0\left(-\frac{\mathbf{k} \cdot \mathbf{q}}{6\alpha^2}, P_f \cdot k\right) \\
 &+ \left\{ -\frac{ia}{24m_q^2} \boldsymbol{\sigma} \cdot (\boldsymbol{\epsilon} \times \mathbf{k}) \boldsymbol{\epsilon}_v \cdot \mathbf{k} - \frac{ib' \omega}{12m_q \alpha^2} \boldsymbol{\sigma} \cdot (\mathbf{q} \times \boldsymbol{\epsilon}_v) \boldsymbol{\epsilon} \cdot \mathbf{q} - g'_v \frac{a\omega}{6\alpha^2} \boldsymbol{\epsilon} \cdot \mathbf{q} \mathbf{A} \cdot \boldsymbol{\epsilon}_v - g'_v \frac{a\omega}{12m_q} \boldsymbol{\epsilon} \cdot \boldsymbol{\epsilon}_v \right\} F^1\left(-\frac{\mathbf{k} \cdot \mathbf{q}}{6\alpha^2}, P_f \cdot k\right) \\
 &- g'_v \frac{a\omega}{72m_q \alpha^2} \boldsymbol{\epsilon}_v \cdot \mathbf{k} \boldsymbol{\epsilon} \cdot \mathbf{q} F^2\left(-\frac{\mathbf{k} \cdot \mathbf{q}}{6\alpha^2}, P_f \cdot k\right). \tag{46}
 \end{aligned}$$

The g -factors in Eqs. (41)–(46) are defined as

$$\langle N_f | \sum_j \hat{I}_j \boldsymbol{\sigma}_j | N_i \rangle = g_A \langle N_f | \boldsymbol{\sigma} | N_i \rangle, \tag{47}$$

$$g_3^u = \langle N_f | \sum_j e_j \hat{I}_j \boldsymbol{\sigma}_j^z | N_i \rangle / g_A, \tag{48}$$

$$g_2^u = \langle N_f | \sum_{i \neq j} e_j \hat{I}_i \boldsymbol{\sigma}_i^z | N_i \rangle / g_A, \tag{49}$$

$$g_v = \langle N_f | \sum_j e_j \hat{I}_j | N_i \rangle / g_3^u g_A, \tag{50}$$

$$g'_v = \frac{1}{3g_2^u g_A} \langle N_f | \sum_{i \neq j} \hat{I}_i e_j \boldsymbol{\sigma}_i \cdot \boldsymbol{\sigma}_j | N_i \rangle, \tag{51}$$

$$g'_a = \frac{1}{2g_2^u g_A} \langle N_f | \sum_{i \neq j} \hat{I}_i e_j (\boldsymbol{\sigma}_i \times \boldsymbol{\sigma}_j)_z | N_i \rangle. \tag{52}$$

The numerical values of these g -factors have been derived in Ref. [11] in the $SU(6) \otimes O(3)$ symmetry limit; they are listed in Table I for completeness.

The first terms of Eq. (45) and Eq. (46) correspond to the correlation between the magnetic transition and the c.m. motion of the meson transition operator and they contribute to the leading Born term in the u-channel. The second terms are due to correlations between the internal and c.m. motion of the photon and meson transition operators, and they only contribute to the transitions between the ground and $n \geq 1$ excited states in the harmonic oscillator basis. The last terms in both equations represent the correlation of the internal motion between the photon and meson transition operators, which only contribute to transitions between the ground and $n \geq 2$ excited states.

As pointed out before, the mass splitting between the ground state spin 1/2 and spin 3/2 is significant, the transition amplitudes for Δ resonance in ρ production or Σ^* resonance

in K^* production have to be computed separately. The transition amplitude with $n=0$ corresponding to the correlation of magnetic transitions is

$$\begin{aligned}
 M^u(n=0) &= -\frac{1}{2m_q} \frac{M_f e^{-(q^2+k^2)/6\alpha^2}}{P_f \cdot k + \delta M^2/2} \frac{b'}{2m_q} \\
 &\times [(g_3^u g_v + g_2^u g'_v)(\mathbf{k} \times \boldsymbol{\epsilon}) \cdot (\mathbf{q} \times \boldsymbol{\epsilon}_v) \\
 &+ i(g_3^u - g_2^u g'_a) \boldsymbol{\sigma} \cdot (\mathbf{k} \times \boldsymbol{\epsilon}) \times (\mathbf{q} \times \boldsymbol{\epsilon}_v)]. \tag{53}
 \end{aligned}$$

The amplitude for spin 1/2 intermediate states in the total $n=0$ amplitudes is

$$\begin{aligned}
 &\langle N_f | h_e | N(J=1/2) \rangle \langle N(J=1/2) | H_m | N_i \rangle \\
 &= \frac{\mu_N b'}{2m_q} \frac{M_f e^{-(q^2+k^2)/6\alpha^2}}{P_f \cdot k + \delta M^2/2} [(\mathbf{k} \times \boldsymbol{\epsilon}) \cdot (\mathbf{q} \times \boldsymbol{\epsilon}_v) \\
 &+ i \boldsymbol{\sigma} \cdot (\mathbf{k} \times \boldsymbol{\epsilon}) \times (\mathbf{q} \times \boldsymbol{\epsilon}_v)], \tag{54}
 \end{aligned}$$

where μ_N is the magnetic moment, which has the following values for different processes:

$$\mu_N = \begin{cases} \mu_\Lambda + \frac{g_{K^* \Sigma N}}{g_{K^* \Lambda N}} \mu_{\Lambda \Sigma} & \text{for } \gamma N \rightarrow K^* \Lambda \\ \mu_{\Sigma^0} + \frac{g_{K^* \Lambda N}}{g_{K^* \Sigma N}} \mu_{\Lambda \Sigma} & \text{for } \gamma N \rightarrow K^* \Sigma \\ \mu_{N_f} & \text{for } \gamma N \rightarrow \rho N_f. \end{cases} \tag{55}$$

Thus, we obtain the spin 3/2 resonance contribution to the transition amplitude by subtracting the spin 1/2 intermediate state contributions from the total $n=0$ amplitudes as follows:

TABLE I. The g -factors in the u -channel amplitudes in Eqs. (45) and (46) for different production processes.

Reactions	g_3^u	g_2^u	g_v	g_v'	g_a'	g_A	g_S	g_v'
$\gamma p \rightarrow \omega p$	1	0	1	0	0	1	0	3
$\gamma n \rightarrow \omega n$	$-\frac{2}{3}$	$\frac{2}{3}$	0	-1	0	1	0	3
$\gamma p \rightarrow \rho^+ n$	$-\frac{1}{3}$	$\frac{1}{3}$	$\frac{3}{5}$	$\frac{1}{5}$	$\frac{9}{5}$	$\frac{5}{3}$	$-\frac{2\mu_n}{5}$	1
$\gamma n \rightarrow \rho^- p$	$\frac{2}{3}$	$\frac{1}{3}$	$\frac{3}{5}$	$\frac{1}{5}$	$-\frac{9}{5}$	$-\frac{5}{3}$	$-\frac{4\mu_p}{15}$	1
$\gamma p \rightarrow \rho^0 p$	$\frac{7}{15}$	$\frac{8}{15}$	$\frac{15}{7}$	2	0	$\frac{5}{3\sqrt{2}}$	$\frac{8\mu_p}{15}$	$-\frac{1}{\sqrt{2}}$
$\gamma n \rightarrow \rho^0 n$	$-\frac{2}{15}$	$\frac{2}{15}$	6	-7	0	$-\frac{5}{3\sqrt{2}}$	$\frac{4\mu_n}{5}$	$\frac{1}{\sqrt{2}}$
$\gamma p \rightarrow K^{*+} \Lambda$	$-\frac{1}{3}$	$\frac{1}{3}$	1	1	1	$\sqrt{\frac{3}{2}}$	$-\frac{\mu_\Lambda}{3}$	$\sqrt{\frac{3}{2}}$
$\gamma n \rightarrow K^{*0} \Lambda$	$-\frac{1}{3}$	$\frac{1}{3}$	1	-1	-1	$\sqrt{\frac{3}{2}}$	$\frac{\mu_\Lambda}{3}$	$\sqrt{\frac{3}{2}}$
$\gamma p \rightarrow K^{*+} \Sigma^0$	$-\frac{1}{3}$	$\frac{1}{3}$	-3	-7	9	$-\frac{1}{3\sqrt{2}}$	μ_{Σ^0}	$\frac{1}{\sqrt{2}}$
$\gamma n \rightarrow K^{*0} \Sigma^0$	$-\frac{1}{3}$	$\frac{1}{3}$	-3	11	-9	$\frac{1}{3\sqrt{2}}$	μ_{Σ^0}	$-\frac{1}{\sqrt{2}}$
$\gamma p \rightarrow K^{*0} \Sigma^+$	$-\frac{1}{3}$	$\frac{4}{3}$	-3	2	0	$\frac{1}{3}$	$\frac{2\mu_{\Sigma^+}}{3}$	0
$\gamma n \rightarrow K^{*+} \Sigma^-$	$-\frac{1}{3}$	$-\frac{2}{3}$	-3	2	0	$-\frac{1}{3}$	0	1
$\gamma p \rightarrow \phi p$	1	0	1	0	0	1	0	3
$\gamma n \rightarrow \phi n$	$-\frac{2}{3}$	$\frac{2}{3}$	0	-1	0	1	0	3

$$\begin{aligned}
M^u = & -\frac{b'}{2m_q} \frac{M_f e^{-(q^2+k^2)/6\alpha^2}}{P_f \cdot k + \delta M^2/2} \{ [(g_3^u g_v + g_2^u g_v')/2m_q - \mu_N] \\
& \times (\mathbf{k} \times \boldsymbol{\epsilon}) \cdot (\mathbf{q} \times \boldsymbol{\epsilon}_v) + i[(g_3^u - g_2^u g_a')/2m_q - \mu_N] \\
& \times \boldsymbol{\sigma} \cdot [(\mathbf{k} \times \boldsymbol{\epsilon}) \times (\mathbf{q} \times \boldsymbol{\epsilon}_v)] \}. \quad (56)
\end{aligned}$$

Substituting the g -factor coefficients into the above equation gives the following general expression for spin 3/2 resonance with $n=0$:

$$\begin{aligned}
M^u = & -\frac{b'}{2m_q} \frac{M_f g_s e^{-(q^2+k^2)/6\alpha^2}}{M_N (P_f \cdot k + \delta M^2/2)} \{ 2\boldsymbol{\sigma} \cdot (\mathbf{q} \times \boldsymbol{\epsilon}_v) \boldsymbol{\sigma} \cdot (\mathbf{k} \times \boldsymbol{\epsilon}) \\
& - i\boldsymbol{\sigma} \cdot [(\mathbf{q} \times \boldsymbol{\epsilon}_v) \times (\mathbf{k} \times \boldsymbol{\epsilon})] \}, \quad (57)
\end{aligned}$$

where the value of g_s is given in Table I.

Note that the transition amplitudes here are generally written as operators that are similar to the CGLN amplitudes in pseudoscalar meson photoproduction. They have to be transformed into the helicity amplitudes defined in Eq. (4). In Tables II and III, we show the relations between the operators presented here and the helicity amplitudes; they are generally related by the Wigner d -function.

TABLE II. The operators in the longitudinal excitations expressed in terms of the helicity amplitudes. $\hat{\mathbf{k}}$ and $\hat{\mathbf{q}}$ are the unit vectors of \mathbf{k} and \mathbf{q} , respectively. The d functions depend on the rotation angle θ between \mathbf{k} and \mathbf{q} . All other components of $H_{a\lambda_V}$ are zero. $\lambda_2 = \pm \frac{1}{2}$ denotes the helicity of the final state nucleon.

Operators	$H_{10}(\lambda_2 = \frac{1}{2})$ $H_{30}(\lambda_2 = -\frac{1}{2})$	$H_{20}(\lambda_2 = \frac{1}{2})$ $H_{40}(\lambda_2 = -\frac{1}{2})$
$\hat{\mathbf{q}} \cdot \boldsymbol{\epsilon}$	$d_{10}^1 d_{-1/2\lambda_2}^{1/2}$	$d_{10}^1 d_{1/2\lambda_2}^{1/2}$
$\boldsymbol{\sigma} \cdot (\boldsymbol{\epsilon} \times \hat{\mathbf{k}})$	$i\sqrt{2} d_{1/2\lambda_2}^{1/2}$	0
$\boldsymbol{\sigma} \cdot (\boldsymbol{\epsilon} \times \hat{\mathbf{q}})$	$i d_{10}^1 d_{-1/2\lambda_2}^{1/2}$ $+ i\sqrt{2} d_{00}^1 d_{1/2\lambda_2}^{1/2}$	$-i d_{10}^1 d_{1/2\lambda_2}^{1/2}$
$(\boldsymbol{\epsilon} \times \hat{\mathbf{k}}) \cdot \hat{\mathbf{q}} \boldsymbol{\sigma} \cdot \hat{\mathbf{q}}$	$i\sqrt{2} d_{10}^1 d_{10}^1 d_{1/2\lambda_2}^{1/2}$	$i\sqrt{2} d_{10}^1 d_{-10}^1 d_{-1/2\lambda_2}^{1/2}$
$(\boldsymbol{\epsilon} \times \hat{\mathbf{k}}) \cdot \hat{\mathbf{q}} \boldsymbol{\sigma} \cdot \hat{\mathbf{k}}$	$-i d_{10}^1 d_{-1/2\lambda_2}^{1/2}$	$i d_{10}^1 d_{1/2\lambda_2}^{1/2}$

C. S-channel transition amplitudes

The third term in Eq. (29) and second term in Eq. (38) are the s -channel longitudinal and transverse transition amplitudes. Following the derivation for Compton scattering in Ref. [22], we obtain the general transition amplitude for excited states in the s -channel,

$$H_{a\lambda_V}^J = \frac{2M_R}{s - M_R(M_R - i\Gamma(\mathbf{q}))} h_{a\lambda_V}^J, \quad (58)$$

where $\sqrt{s} = E_i + \omega = E_f + \omega_m$ is the total energy of the system, and $H_{a\lambda_V}^J$ are the helicity amplitudes defined previously. $\Gamma(\mathbf{q})$ in Eq. (58) denotes the total width of the resonance, which is a function of the final state momentum \mathbf{q} . For a resonance decaying into a two-body final state with relative angular momentum l , the decay width $\Gamma(\mathbf{q})$ is given by

$$\Gamma(\mathbf{q}) = \Gamma_R \frac{\sqrt{s}}{M_R} \sum_i x_i \left(\frac{|\mathbf{q}_i|}{|\mathbf{q}_i^R|} \right)^{2l+1} \frac{D_l(\mathbf{q}_i)}{D_l(\mathbf{q}_i^R)}, \quad (59)$$

with

$$|\mathbf{q}_i^R| = \sqrt{\frac{(M_R^2 - M_N^2 + M_i^2)^2}{4M_R^2} - M_i^2}, \quad (60)$$

and

$$|\mathbf{q}_i| = \sqrt{\frac{(s - M_N^2 + M_i^2)^2}{4s} - M_i^2}, \quad (61)$$

where x_i is the branching ratio of the resonance decaying into a meson with mass M_i and a nucleon, and Γ_R is the total decay width of the resonance with the mass M_R . The function $D_l(\mathbf{q})$ in Eq. (59), called fission barrier [23], is wavefunction dependent and has the following form in the harmonic oscillator basis:

$$D_l(\mathbf{q}) = \exp\left(-\frac{\mathbf{q}^2}{3\alpha^2}\right), \quad (62)$$

TABLE III. The operators in the transverse excitations expressed in terms of the helicity amplitudes. $\hat{\mathbf{k}}$ and $\hat{\mathbf{q}}$ are the unit vectors of \mathbf{k} and \mathbf{q} , respectively. The d functions depend on the rotation angle θ between \mathbf{k} and \mathbf{q} . $\lambda_V = \pm 1$ denotes the helicity of ω meson, and $\lambda_2 = \pm \frac{1}{2}$ denotes the helicity of the final nucleon.

Operators	$H_{1\lambda_V}(\lambda_2 = \frac{1}{2})$	$H_{2\lambda_V}(\lambda_2 = \frac{1}{2})$
	$H_{3\lambda_V}(\lambda_2 = -\frac{1}{2})$	$H_{4\lambda_V}(\lambda_2 = -\frac{1}{2})$
$(\boldsymbol{\epsilon} \times \hat{\mathbf{k}}) \cdot (\boldsymbol{\epsilon}_v \times \hat{\mathbf{q}})$	$-\lambda_V d_{1\lambda_V}^1 d_{-1/2\lambda_2}^{1/2}$	$-\lambda_V d_{1\lambda_V}^1 d_{-1/2\lambda_2}^{1/2}$
$\boldsymbol{\sigma} \cdot \hat{\mathbf{Z}}$	$-i\lambda_V d_{1\lambda_V}^1 d_{-1/2\lambda_2}^{1/2}$ $-i\sqrt{2}\lambda_V d_{0\lambda_V}^1 d_{1/2\lambda_2}^{1/2}$	$i\lambda_V d_{1\lambda_V}^1 d_{1/2\lambda_2}^{1/2}$
$\boldsymbol{\sigma} \cdot (\boldsymbol{\epsilon} \times \hat{\mathbf{k}}) \hat{\mathbf{k}} \cdot \boldsymbol{\epsilon}_v$	$i\sqrt{2}d_{0\lambda_V}^1 d_{1/2\lambda_2}^{1/2}$	0
$\boldsymbol{\sigma} \cdot (\boldsymbol{\epsilon}_v \times \hat{\mathbf{q}}) \hat{\mathbf{q}} \cdot \boldsymbol{\epsilon}$	$i\sqrt{2}\lambda_V d_{10}^1 d_{1\lambda_V}^1 d_{1/2\lambda_2}^{1/2}$ $-i\lambda_V d_{10}^1 d_{0\lambda_V}^1 d_{-1/2\lambda_2}^{1/2}$	$i\sqrt{2}\lambda_V d_{10}^1 d_{-1\lambda_V}^1 d_{-1/2\lambda_2}^{1/2}$ $+i\lambda_V d_{10}^1 d_{0\lambda_V}^1 d_{1/2\lambda_2}^{1/2}$
$\boldsymbol{\epsilon}_v \cdot \boldsymbol{\epsilon}$	$d_{1\lambda_V}^1 d_{-1/2\lambda_2}^{1/2}$	$d_{1\lambda_V}^1 d_{1/2\lambda_2}^{1/2}$
$\hat{\mathbf{q}} \cdot \boldsymbol{\epsilon} \hat{\mathbf{k}} \cdot \boldsymbol{\epsilon}_v$	$d_{0\lambda_V}^1 d_{01}^1 d_{-1/2\lambda_2}^{1/2}$	$d_{0\lambda_V}^1 d_{01}^1 d_{1/2\lambda_2}^{1/2}$
$\boldsymbol{\sigma} \cdot (\boldsymbol{\epsilon} \times \hat{\mathbf{q}}) \hat{\mathbf{k}} \cdot \boldsymbol{\epsilon}_v$	$i\sqrt{2}d_{00}^1 d_{0\lambda_V}^1 d_{1/2\lambda_2}^{1/2}$ $+id_{10}^1 d_{0\lambda_V}^1 d_{1/2\lambda_2}^{1/2}$	$-id_{10}^1 d_{0\lambda_V}^1 d_{1/2\lambda_2}^{1/2}$
$\boldsymbol{\sigma} \cdot (\boldsymbol{\epsilon}_v \times \hat{\mathbf{q}}) \hat{\mathbf{q}} \cdot \boldsymbol{\epsilon}$	$-i\sqrt{2}d_{10}^1 d_{-1\lambda_V}^1 d_{1/2\lambda_2}^{1/2}$	$-i\sqrt{2}d_{10}^1 d_{1\lambda_V}^1 d_{-1/2\lambda_2}^{1/2}$
$\boldsymbol{\sigma} \cdot (\boldsymbol{\epsilon}_v \times \boldsymbol{\epsilon})$	$-i\sqrt{2}d_{0\lambda_V}^1 d_{1/2\lambda_2}^{1/2}$ $-id_{1\lambda_V}^1 d_{-1/2\lambda_2}^{1/2}$	$id_{1\lambda_V}^1 d_{1/2\lambda_2}^{1/2}$
$\boldsymbol{\sigma} \cdot (\hat{\mathbf{k}} \times \hat{\mathbf{q}}) \boldsymbol{\epsilon} \cdot \boldsymbol{\epsilon}_v$	$i\sqrt{2}d_{-10}^1 d_{1\lambda_V}^1 d_{1/2\lambda_2}^{1/2}$	$i\sqrt{2}d_{10}^1 d_{1\lambda_V}^1 d_{-1/2\lambda_2}^{1/2}$
$(\boldsymbol{\epsilon} \times \boldsymbol{\epsilon}_v) \cdot \hat{\mathbf{q}} \boldsymbol{\sigma} \cdot \hat{\mathbf{q}}$	$i\sqrt{2}\lambda_V d_{1\lambda_V}^1 d_{10}^1 d_{1/2\lambda_2}^{1/2}$ $-i\lambda_V d_{1\lambda_V}^1 d_{00}^1 d_{-1/2\lambda_2}^{1/2}$	$i\sqrt{2}\lambda_V d_{1\lambda_V}^1 d_{-10}^1 d_{-1/2\lambda_2}^{1/2}$ $+i\lambda_V d_{1\lambda_V}^1 d_{00}^1 d_{1/2\lambda_2}^{1/2}$
$(\boldsymbol{\epsilon} \times \boldsymbol{\epsilon}_v) \cdot \hat{\mathbf{q}} \boldsymbol{\sigma} \cdot \hat{\mathbf{k}}$	$-i\lambda_V d_{1\lambda_V}^1 d_{-1/2\lambda_2}^{1/2}$	$i\lambda_V d_{1\lambda_V}^1 d_{1/2\lambda_2}^{1/2}$
$(\boldsymbol{\epsilon} \times \boldsymbol{\epsilon}_v) \cdot \hat{\mathbf{k}} \boldsymbol{\sigma} \cdot \hat{\mathbf{q}}$	$i\sqrt{2}d_{1\lambda_V}^1 d_{10}^1 d_{1/2\lambda_2}^{1/2}$ $-id_{1\lambda_V}^1 d_{00}^1 d_{-1/2\lambda_2}^{1/2}$	$i\sqrt{2}d_{1\lambda_V}^1 d_{-10}^1 d_{-1/2\lambda_2}^{1/2}$ $+id_{1\lambda_V}^1 d_{00}^1 d_{1/2\lambda_2}^{1/2}$
$(\boldsymbol{\epsilon} \times \boldsymbol{\epsilon}_v) \cdot \hat{\mathbf{k}} \boldsymbol{\sigma} \cdot \hat{\mathbf{k}}$	$-id_{1\lambda_V}^1 d_{-1/2\lambda_2}^{1/2}$	$id_{1\lambda_V}^1 d_{1/2\lambda_2}^{1/2}$

which is independent of l . In principle, the branching ratio x_i should also be evaluated in the quark model.

For a given intermediate resonance state with spin J , the twelve independent helicity amplitudes $h_{a\lambda_V}^J$ in Eq. (58) are a combination of the meson and photon helicity amplitudes together with the Wigner- d functions

$$h_{a\lambda_V}^J = \sum_{\Lambda_f} d_{\Lambda_f}^J(\theta) A_{\Lambda_f}^V A_{\Lambda_i}^\gamma, \quad (63)$$

where $\Lambda_f = \lambda_V - \lambda_2$, $\Lambda_i = \lambda - \lambda_1$ and $\mathbf{k} \cdot \mathbf{q} = |\mathbf{k}||\mathbf{q}|\cos(\theta)$.

The $A_{1/2}^\gamma$ and $A_{3/2}^\gamma$ in Eq. (63) represent the helicity amplitudes in the s-channel for the photon interactions; their explicit expressions have been given in Ref. [24].

More explicitly, the 12 independent helicity amplitudes are related to the photon helicity amplitudes $A_{1/2}^\gamma$, $A_{3/2}^\gamma$ and vector meson helicity amplitudes $S_{1/2}^V$, $A_{1/2}^V$, and $A_{3/2}^V$ through the following relations:

TABLE IV. The angular momentum and flavor parts of the helicity amplitudes for $\gamma p \rightarrow \omega p(\phi p)$, or $\gamma n \rightarrow \omega n(\phi n)$, in the $SU(6) \otimes O(3)$ symmetry limit. They are the coefficients of the spatial integrals A , B , and S in Eqs. (71) and (72). The analytic expressions for A , B , and S in Tables IV–VI are given in Table VII. The asterisk in Tables IV–VI denotes those states decoupling in spin and flavor space, thus, their amplitudes are zero.

States	$S_{1/2}$	$A_{1/2}$		$A_{3/2}$	
	S	A	B	A	B
$N(^2P_M)_{1/2^-}$	0	0	$-\frac{2}{3\sqrt{6}}$	0	0
$N(^2P_M)_{3/2^-}$	0	0	$\frac{2}{3\sqrt{3}}$	0	0
$N(^4P_M)_{1/2^-}$	0	0	$-\frac{1}{3\sqrt{6}}$	*	*
$N(^4P_M)_{3/2^-}$	0	0	$\frac{1}{3\sqrt{30}}$	0	$-\frac{1}{\sqrt{15}}$
$N(^4P_M)_{5/2^-}$	0	0	$\frac{1}{\sqrt{30}}$	0	$\frac{1}{\sqrt{10}}$
$N(^2D_S)_{3/2^+}$	$-\sqrt{\frac{2}{5}}$	$\sqrt{\frac{3}{5}}$	$-\frac{1}{3}\sqrt{\frac{2}{5}}$	$-\frac{1}{\sqrt{5}}$	*
$N(^2D_S)_{5/2^+}$	$\sqrt{\frac{3}{5}}$	$\sqrt{\frac{2}{5}}$	$\frac{1}{3}\sqrt{\frac{3}{5}}$	$\frac{2}{\sqrt{5}}$	*
$N(^2S'_S)_{1/2^+}$	1	*	$\frac{1}{3}$	*	*
$N(^2S_M)_{1/2^+}$	0	*	$\frac{2}{3\sqrt{2}}$	*	*
$N(^4S_M)_{3/2^+}$	0	*	$\frac{1}{3\sqrt{2}}$	*	$\frac{1}{\sqrt{6}}$
$N(^2D_M)_{3/2^+}$	0	0	$-\frac{2}{3\sqrt{5}}$	0	*
$N(^2D_M)_{5/2^+}$	0	0	$\sqrt{\frac{2}{15}}$	0	*
$N(^4D_M)_{1/2^+}$	0	0	$\frac{1}{3\sqrt{10}}$	*	*
$N(^4D_M)_{3/2^+}$	0	0	$-\frac{1}{3\sqrt{10}}$	0	$\frac{1}{\sqrt{30}}$
$N(^4D_M)_{5/2^+}$	0	0	$-\frac{1}{\sqrt{210}}$	0	$-\sqrt{\frac{3}{35}}$
$N(^4D_M)_{7/2^+}$	0	0	$\frac{1}{\sqrt{35}}$	0	$\frac{1}{\sqrt{21}}$

$$h_{11}^J = d_{1/2,3/2}^J(\theta) A_{1/2}^V A_{3/2}^\gamma,$$

$$h_{10}^J = d_{-1/2,3/2}^J(\theta) S_{-1/2}^V A_{3/2}^\gamma,$$

$$h_{1-1}^J = d_{-3/2,3/2}^J(\theta) A_{-3/2}^V A_{3/2}^\gamma \quad (64)$$

for $a=1$, and $\lambda_V=1,0,-1$,

$$\begin{aligned} h_{21}^J &= d_{1/2,1/2}^J(\theta) A_{1/2}^V A_{1/2}^\gamma, \\ h_{20}^J &= d_{-1/2,1/2}^J(\theta) S_{-1/2}^V A_{1/2}^\gamma, \\ h_{2-1}^J &= d_{-3/2,1/2}^J(\theta) A_{-3/2}^V A_{1/2}^\gamma \end{aligned} \quad (65)$$

for $a=2$, and $\lambda_V=1,0,-1$,

$$\begin{aligned} h_{31}^J &= d_{3/2,3/2}^J(\theta) A_{3/2}^V A_{3/2}^\gamma, \\ h_{30}^J &= d_{1/2,3/2}^J(\theta) S_{1/2}^V A_{3/2}^\gamma, \\ h_{3-1}^J &= d_{-1/2,3/2}^J(\theta) A_{-1/2}^V A_{3/2}^\gamma \end{aligned} \quad (66)$$

for $a=3$, and $\lambda_V=1,0,-1$, and

$$\begin{aligned} h_{41}^J &= d_{3/2,1/2}^J(\theta) A_{3/2}^V A_{1/2}^\gamma, \\ h_{40}^J &= d_{1/2,1/2}^J(\theta) S_{1/2}^V A_{1/2}^\gamma, \\ h_{4-1}^J &= d_{-1/2,1/2}^J(\theta) A_{-1/2}^V A_{1/2}^\gamma \end{aligned} \quad (67)$$

for $a=4$, and $\lambda_V=1,0,-1$.

The amplitudes with negative helicities in the above equations are not independent from those with positive ones; they are related by an additional phase factor according to the Wigner-Eckart theorem,

$$A_{-\lambda}^V = (-1)^{J_f - J_i - J_V} A_{\lambda}^V, \quad (68)$$

where J_f and J_i are the final nucleon and initial resonance spins, and J_V is the angular momentum of the vector meson. The angular distributions of the helicity amplitudes in terms of the multipole transitions have been discussed in Ref. [25], and the expressions here are consistent with their analysis.

The evaluation of the vector meson helicity amplitudes are similar to that of the photon amplitudes. The transition operator for a resonance decaying into a vector meson and a nucleon is

$$H_m^T = \sum_l \left\{ i \frac{b'}{2m_q} \boldsymbol{\sigma}_l \cdot (\mathbf{q} \times \boldsymbol{\epsilon}_v) + \frac{a}{2\mu_q} \mathbf{p}_l' \cdot \boldsymbol{\epsilon}_v \right\} \hat{I}_l e^{-i\mathbf{q} \cdot \mathbf{r}_l}, \quad (69)$$

for transverse transitions and

$$H_m^L = \frac{a\mu}{|\mathbf{q}|} \sum_l \hat{I}_l e^{-i\mathbf{q} \cdot \mathbf{r}_l} \quad (70)$$

for longitudinal transitions. Thus, H_m^T and H_m^L have the group structure,

$$H_m^T = \hat{I}_3 (A L_{(3)}^- + B \sigma_{(3)}^-), \quad (71)$$

and

$$H_m^L = \hat{I}_3 S, \quad (72)$$

where

$$A = \frac{3a}{2\sqrt{2}m_q} \langle \psi_f | p_3^- e^{-i\mathbf{q} \cdot \mathbf{r}_3} | \psi_R \rangle, \quad (73)$$

$$B = \frac{-3b'}{2m_q} |\mathbf{q}| \langle \psi_f | e^{-i\mathbf{q} \cdot \mathbf{r}_3} | \psi_R \rangle, \quad (74)$$

$$S = -\frac{3\mu a}{|\mathbf{q}|} \langle \psi_f | e^{-i\mathbf{q} \cdot \mathbf{r}_3} | \psi_R \rangle, \quad (75)$$

where $p_3^- = p_x - ip_y$. In Eq. (71), $L_{(3)}^-$ and $\sigma_{(3)}^-$ denote orbital and spin flip operators. The helicity amplitudes $A_{1/2}^V$, $A_{3/2}^V$, and $S_{1/2}^V$ are the matrix elements of Eq. (71) and Eq. (72). We list the angular momentum and flavor parts of $A_{1/2}^V$, $A_{3/2}^V$, and $S_{1/2}^V$ for ω and ρ photoproduction in Tables IV–VI in the $SU(6) \otimes O(3)$ limit with A , B , and S in the second row to denote the corresponding spatial integrals, which are given in Table VII.

The resonances with $n \geq 3$ are treated as degenerate since there is little information available about them. Their longitudinal transition in the s -channel is given by

$$h_{a\lambda_V=0}^J = (M_3^s(L) + M_2^s(L)) e^{-(\mathbf{q}^2 + \mathbf{k}^2)/6\alpha^2} \quad (76)$$

where

$$\begin{aligned} M_3^s(L) &= g_3^s \frac{a\mu}{|\mathbf{q}|} \left\{ -\frac{i}{2m_q} \boldsymbol{\sigma} \cdot (\boldsymbol{\epsilon} \times \mathbf{k}) \frac{1}{n!} \left(\frac{\mathbf{k} \cdot \mathbf{q}}{3\alpha^2} \right)^n \right. \\ &\quad \left. + g_v \frac{\omega}{3\alpha^2} \mathbf{q} \cdot \boldsymbol{\epsilon} \frac{1}{(n-1)!} \left(\frac{\mathbf{k} \cdot \mathbf{q}}{3\alpha^2} \right)^{n-1} \right\}, \end{aligned} \quad (77)$$

and

$$\begin{aligned} M_2^s(L) &= -g_2^u \frac{a\mu}{|\mathbf{q}|} \left\{ g_a' \frac{i}{2m_q} \boldsymbol{\sigma} \cdot (\boldsymbol{\epsilon} \times \mathbf{k}) \frac{1}{n!} \left(\frac{-\mathbf{k} \cdot \mathbf{q}}{6\alpha^2} \right)^n \right. \\ &\quad \left. + g_v' \frac{\omega}{6\alpha^2} \mathbf{q} \cdot \boldsymbol{\epsilon} \frac{1}{(n-1)!} \left(\frac{-\mathbf{k} \cdot \mathbf{q}}{6\alpha^2} \right)^{n-1} \right\}. \end{aligned} \quad (78)$$

The g -factors in Eqs. (77) and (78) have been defined previously, and

$$g_3^s = \langle N_f | \sum_j \hat{I}_j e_j \sigma_j^z | N_i \rangle / g_A = e_m + g_3^u, \quad (79)$$

where e_m is the charge of the outgoing vector meson.

The transverse transition amplitudes at the quark level are

$$h_{a\lambda_V=\pm 1}^J = (M_3^s(T) + M_2^s(T)) e^{-(\mathbf{q}^2 + \mathbf{k}^2)/6\alpha^2}, \quad (80)$$

where

TABLE V. The angular momentum and flavor parts of the helicity amplitudes for $\gamma p \rightarrow \rho^0 p$ in the $SU(6) \otimes O(3)$ symmetry limit, while those for $\gamma n \rightarrow \rho^0 n$ are given by $A(\gamma n \rightarrow \rho^0 n) = (-1)^{I+1/2} A(\gamma p \rightarrow \rho^0 p)$, where I is the isospin of the resonances.

States	$S_{1/2}$			$A_{1/2}$		$A_{3/2}$		States	$S_{1/2}$			$A_{1/2}$		$A_{3/2}$	
	S	A	B	A	B	A	B		S	A	B	A	B		
$N(2P_M)_{1/2^-}$	$\frac{1}{3\sqrt{3}}$	$-\frac{\sqrt{2}}{3\sqrt{3}}$	$\frac{2}{9\sqrt{3}}$	*	*			$N(2S_M)_{1/2^+}$	$-\frac{1}{3}$	*	$-\frac{2}{9}$	*	*		
$N(2P_M)_{3/2^-}$	$-\frac{1}{3}\sqrt{\frac{2}{3}}$	$-\frac{1}{3\sqrt{3}}$	$-\frac{2}{9}\sqrt{\frac{2}{3}}$	$-\frac{1}{3}$	*			$\Delta(4S'_S)_{3/2}$	0	*	$\frac{2}{9}$	*	$\frac{2}{3\sqrt{3}}$		
$N(4P_M)_{1/2^-}$	0	0	$-\frac{1}{18\sqrt{3}}$	*	*			$\Delta(4S_S)_{3/2}$	0	*	$\frac{2}{9}$	*	$\frac{2}{3\sqrt{3}}$		
$N(4P_M)_{3/2^-}$	0	0	$\frac{1}{18\sqrt{15}}$	0	$\frac{1}{6\sqrt{5}}$			$N(2S_M)_{1/2^+}$	$-\frac{1}{3}$	*	$-\frac{2}{9}$	*	*		
$N(4P_M)_{5/2^-}$	0	0	$\frac{1}{6\sqrt{15}}$	0	$\frac{1}{\sqrt{30}}$			$N(4S_M)_{3/2^+}$	0	*	$\frac{1}{18}$	*	$\frac{1}{6\sqrt{3}}$		
$\Delta(2P_M)_{1/2^-}$	$-\frac{1}{3\sqrt{3}}$	$\frac{1}{3}\sqrt{\frac{2}{3}}$	$\frac{1}{9\sqrt{3}}$	*	*			$\Delta(2S_M)_{1/2^+}$	$\frac{1}{3}$	*	$-\frac{1}{9}$	*	*		
$\Delta(2P_M)_{3/2^-}$	$\frac{1}{3}\sqrt{\frac{2}{3}}$	$\frac{1}{3\sqrt{3}}$	$-\frac{1}{9}\sqrt{\frac{2}{3}}$	$\frac{1}{3}$	*			$N(2D_M)_{3/2^+}$	$\frac{1}{3}\sqrt{\frac{2}{5}}$	$-\frac{1}{3}\sqrt{\frac{3}{5}}$	$\frac{2}{9}\sqrt{\frac{2}{5}}$	$\frac{1}{3\sqrt{5}}$	*		
$N(2D_S)_{3/2^+}$	$\frac{1}{3\sqrt{5}}$	$-\frac{1}{\sqrt{30}}$	$\frac{\sqrt{5}}{9}$	$\frac{1}{3\sqrt{10}}$	*			$N(2D_M)_{5/2^+}$	$-\frac{1}{3}\sqrt{\frac{3}{5}}$	$-\frac{1}{3}\sqrt{\frac{2}{5}}$	$-\frac{2}{9}\sqrt{\frac{3}{5}}$	$-\frac{2}{3\sqrt{5}}$	*		
$N(2D_S)_{5/2^+}$	$-\frac{1}{\sqrt{30}}$	$-\frac{1}{3\sqrt{5}}$	$-\frac{5}{9}\sqrt{\frac{3}{10}}$	$-\frac{2}{3\sqrt{10}}$	*			$N(4S_M)_{3/2^+}$	0	*	$\frac{1}{18}$	*	$\frac{1}{6\sqrt{3}}$		
$\Delta(4D_S)_{1/2^+}$	0	0	$\frac{2}{9\sqrt{5}}$	*	*			$N(4D_M)_{1/2^+}$	0	0	$\frac{1}{18\sqrt{5}}$	*	*		
$\Delta(4D_S)_{3/2^+}$	0	0	$-\frac{2}{9\sqrt{5}}$	0	$\frac{2}{3\sqrt{15}}$			$N(4D_M)_{3/2^+}$	0	0	$-\frac{1}{18\sqrt{5}}$	0	$\frac{1}{6\sqrt{15}}$		
$\Delta(4D_S)_{5/2^+}$	0	0	$-\frac{2}{9}\sqrt{\frac{3}{35}}$	0	$-\frac{2}{3}\sqrt{\frac{6}{35}}$			$N(4D_M)_{5/2^+}$	0	0	$-\frac{1}{18}\sqrt{\frac{3}{35}}$	0	$-\frac{1}{6}\sqrt{\frac{6}{35}}$		
$\Delta(4D_S)_{7/2^+}$	0	0	$\frac{2}{3}\sqrt{\frac{2}{35}}$	4342				$\Delta(2D_M)_{3/2^+}$	$-\frac{1}{3}\sqrt{2/5}$	$\frac{1}{3}\sqrt{3/5}$	$\frac{1}{9}\sqrt{2/5}$	$-\frac{1}{3\sqrt{5}}$	*		
								$\Delta(2D_M)_{5/2^+}$	$\frac{1}{3}\sqrt{3/5}$	$\frac{1}{3}\sqrt{2/5}$	$-\frac{1}{9}\sqrt{3/5}$	$\frac{2}{3\sqrt{5}}$	*		

$$\begin{aligned}
 M_3^s(T)/g_3^s &= \frac{b'}{4m_q^2} \{g_v(\mathbf{q} \times \boldsymbol{\epsilon}_v) \cdot (\boldsymbol{\epsilon} \times \mathbf{k}) \\
 &+ i\boldsymbol{\sigma} \cdot (\mathbf{q} \times \boldsymbol{\epsilon}_v) \times (\boldsymbol{\epsilon} \times \mathbf{k})\} \frac{1}{n!} \left(\frac{\mathbf{k} \cdot \mathbf{q}}{3\alpha^2}\right)^n \\
 &+ \left\{ -\frac{ia}{12m_q^2} \boldsymbol{\sigma} \cdot (\boldsymbol{\epsilon} \times \mathbf{k}) \boldsymbol{\epsilon}_v \cdot \mathbf{k} + \frac{ib'\omega}{6m_q\alpha^2} \boldsymbol{\sigma} \cdot (\mathbf{q} \times \boldsymbol{\epsilon}_v) \boldsymbol{\epsilon} \cdot \mathbf{q} + g_v \frac{a\omega}{6m_q} \boldsymbol{\epsilon}_v \cdot \boldsymbol{\epsilon} \right\} \frac{1}{(n-1)!} \left(\frac{\mathbf{k} \cdot \mathbf{q}}{3\alpha^2}\right)^{n-1} \\
 &+ g_v \frac{a\omega}{18m_q\alpha^2} \boldsymbol{\epsilon}_v \cdot \mathbf{k} \boldsymbol{\epsilon} \cdot \mathbf{q} \frac{1}{(n-2)!} \left(\frac{\mathbf{k} \cdot \mathbf{q}}{3\alpha^2}\right)^{n-2}, \tag{81}
 \end{aligned}$$

$$\begin{aligned}
 M_2^s(T)/g_2^s &= \frac{b'}{4m_q^2} \{g'_v(\mathbf{q} \times \boldsymbol{\epsilon}_v) \cdot (\boldsymbol{\epsilon} \times \mathbf{k}) \\
 &+ ig'_a \boldsymbol{\sigma} \cdot (\mathbf{q} \times \boldsymbol{\epsilon}_v) \times (\boldsymbol{\epsilon} \times \mathbf{k})\} \frac{1}{n!} \left(\frac{-\mathbf{k} \cdot \mathbf{q}}{6\alpha^2}\right)^n \\
 &+ \left\{ \frac{ia}{24m_q^2} \boldsymbol{\sigma} \cdot (\boldsymbol{\epsilon} \times \mathbf{k}) \boldsymbol{\epsilon}_v \cdot \mathbf{k} - \frac{ib'\omega}{12m_q\alpha^2} \boldsymbol{\sigma} \cdot (\mathbf{q} \times \boldsymbol{\epsilon}_v) \boldsymbol{\epsilon} \cdot \mathbf{q} \right. \\
 &\left. - g'_v \frac{a\omega}{12m_q} \boldsymbol{\epsilon}_v \cdot \boldsymbol{\epsilon} \right\} \frac{1}{(n-1)!} \left(\frac{-\mathbf{k} \cdot \mathbf{q}}{6\alpha^2}\right)^{n-1} \\
 &+ g'_v \frac{a\omega}{72m_q\alpha^2} \boldsymbol{\epsilon}_v \cdot \mathbf{k} \boldsymbol{\epsilon} \cdot \mathbf{q} \frac{1}{(n-2)!} \left(\frac{-\mathbf{k} \cdot \mathbf{q}}{6\alpha^2}\right)^{n-2}. \tag{82}
 \end{aligned}$$

and

(82)

TABLE VI. The angular momentum and flavor parts of the helicity amplitudes for $\gamma p \rightarrow \rho^+ n$ in the $SU(6) \otimes O(3)$ symmetry limit, while those for $\gamma n \rightarrow \rho^- p$ are given by $A(\gamma n \rightarrow \rho^- p) = (-1)^{I+1/2} A(\gamma p \rightarrow \rho^+ n)$, where I is the isospin of the resonances.

States	$S_{1/2}$			$A_{1/2}$		$A_{3/2}$		States	$S_{1/2}$			$A_{1/2}$		$A_{3/2}$	
	S	A	B	A	B	A	B		S	A	B	A	B		
$N(^2P_M)_{1/2^-}$	$-\frac{2}{3\sqrt{6}}$	$\frac{2}{3\sqrt{3}}$	$-\frac{4}{9\sqrt{6}}$	*	*	$\Delta(^4S'_S)_{3/2^+}$	0	*	$\frac{2}{9\sqrt{2}}$	*	$\frac{1}{3}\sqrt{\frac{2}{3}}$				
$N(^2P_M)_{3/2^-}$	$\frac{2}{3\sqrt{3}}$	$\frac{2}{3\sqrt{6}}$	$\frac{4}{9\sqrt{3}}$	$\frac{2}{3\sqrt{2}}$	*	$\Delta(^4S_S)_{3/2^+}$	0	*	$\frac{2}{9\sqrt{2}}$	*	$\frac{1}{3}\sqrt{\frac{2}{3}}$				
$N(^4P_M)_{1/2^-}$	0	0	$\frac{1}{9\sqrt{6}}$	*	*	$N(^2S_M)_{1/2^+}$	$\frac{2}{3\sqrt{2}}$	*	$\frac{4}{9\sqrt{2}}$	*	*				
$N(^4P_M)_{3/2^-}$	0	0	$-\frac{1}{9\sqrt{30}}$	0	$-\frac{1}{3\sqrt{10}}$	$N(^4S_M)_{3/2^+}$	0	*	$-\frac{1}{9\sqrt{2}}$	*	$-\frac{1}{3\sqrt{6}}$				
$N(^4P_M)_{5/2^-}$	0	0	$-\frac{1}{3\sqrt{30}}$	0	$-\frac{1}{3\sqrt{15}}$	$\Delta(^2S_M)_{1/2^+}$	$\frac{1}{3\sqrt{2}}$	*	$-\frac{1}{9\sqrt{2}}$	*	*				
$\Delta(^2P_M)_{1/2^-}$	$-\frac{1}{3\sqrt{6}}$	$\frac{1}{3\sqrt{3}}$	$\frac{1}{9\sqrt{6}}$	*	*	$N(^2D_M)_{3/2^+}$	$-\frac{2}{3}\sqrt{\frac{1}{5}}$	$\sqrt{\frac{2}{15}}$	$-\frac{4}{9\sqrt{5}}$	$-\frac{1}{3}\sqrt{\frac{2}{5}}$	*				
$\Delta(^2P_M)_{3/2^-}$	$\frac{1}{3\sqrt{3}}$	$\frac{1}{3\sqrt{6}}$	$-\frac{1}{9\sqrt{3}}$	$\frac{1}{3\sqrt{2}}$	*	$N(^2D_M)_{5/2^+}$	$\sqrt{\frac{2}{15}}$	$\frac{2}{3\sqrt{5}}$	$\frac{4}{9}\sqrt{\frac{3}{10}}$	$\frac{2}{3}\sqrt{\frac{2}{5}}$	*				
$N(^2D_S)_{3/2^+}$	$-\frac{1}{3}\sqrt{\frac{2}{5}}$	$\frac{1}{3}\sqrt{\frac{3}{5}}$	$-\frac{5}{9}\sqrt{\frac{2}{5}}$	$-\frac{1}{3\sqrt{5}}$	*	$N(^4D_M)_{1/2^+}$	0	0	$-\frac{1}{9\sqrt{10}}$	*	*				
$N(^2D_S)_{5/2^+}$	$\frac{1}{3}\sqrt{\frac{3}{5}}$	$\frac{1}{3}\sqrt{\frac{2}{5}}$	$\frac{5}{9}\sqrt{\frac{3}{5}}$	$\frac{2}{3\sqrt{5}}$	*	$N(^4D_M)_{3/2^+}$	0	0	$\frac{1}{9\sqrt{10}}$	0	$-\frac{1}{3\sqrt{30}}$				
$\Delta(^4D_S)_{1/2^+}$	0	0	$\frac{2}{9\sqrt{10}}$	*	*	$N(^4D_M)_{5/2^+}$	0	0	$\frac{1}{9}\sqrt{\frac{3}{70}}$	0	$\frac{1}{3}\sqrt{\frac{3}{35}}$				
$\Delta(^4D_S)_{3/2^+}$	0	0	$-\frac{2}{9\sqrt{10}}$	0	$\frac{1}{3}\sqrt{\frac{2}{15}}$	$N(^4D_M)_{7/2^+}$	0	0	$-\frac{1}{3\sqrt{35}}$	0	$-\frac{1}{3\sqrt{21}}$				
$\Delta(^4D_S)_{5/2^+}$	0	0	$-\frac{1}{9}\sqrt{\frac{6}{35}}$	0	$-\frac{2}{3}\sqrt{\frac{3}{35}}$	$\Delta(^2D_M)_{3/2^+}$	$-\frac{1}{3\sqrt{5}}$	$\frac{1}{\sqrt{30}}$	$\frac{1}{9\sqrt{5}}$	$-\frac{1}{3\sqrt{10}}$	*				
$\Delta(^4D_S)_{7/2^+}$	0	0	$\frac{2}{3\sqrt{35}}$	0	$\frac{2}{3\sqrt{21}}$	$\Delta(^2D_M)_{5/2^+}$	$\frac{1}{\sqrt{30}}$	$\frac{1}{3\sqrt{5}}$	$-\frac{1}{9}\sqrt{\frac{3}{10}}$	$\frac{1}{3}\sqrt{\frac{2}{5}}$	*				
$N(^2S'_S)_{1/2^+}$	$\frac{1}{3}$	*	$\frac{5}{9}$	*	*										

Qualitatively, we find that the resonances with larger partial waves have larger decay widths into the vector meson and nucleon though this is not as explicit as in the pseudoscalar case [11,26]. Thus, we could use the mass and decay width of the high spin states, such as $G_{17}(2190)$ for $n=3$ states and $H_{19}(2220)$ for $n=4$ states in the ω photoproduction. The relation between these operators and the helicity amplitudes $h_{a\lambda_V}$ has been given in Tables II and III.

IV. THE NUMERICAL RESULTS

Before discussing the details of the ω , ρ , and ϕ productions, it should be pointed out that the nonrelativistic wave function in the quark model becomes more inadequate as the energy of the system increases. A procedure to partly remedy this problem is to introduce the Lorentz boost factor in the spatial integrals that involve the spatial wave functions of

nucleons and baryon resonances,

$$R(q, k) \rightarrow \gamma_q \gamma_k R(q \gamma_q, k \gamma_k), \quad (83)$$

where $\gamma_q = M_f/E_f$ and $\gamma_k = M_i/E_i$. A similar procedure had been used in the numerical evaluation of pseudoscalar meson photoproduction [26]. There are two overall parameters from the quark model formalism; the quark mass m_q and the parameter α related to the harmonic oscillator strength, and we adopt the values commonly used in the quark model approach for these parameters,

$$\begin{aligned} m_q &= 330 \text{ MeV}, \\ \alpha &= 410 \text{ MeV}. \end{aligned} \quad (84)$$

Now, we turn our attention to the details of the ω , ρ^0 , ρ^\pm and ϕ photoproductions.

A. The ω photoproduction

The t-channel exchange of M_{fi}^t in Eq. (14) would correspond to ω exchange which is absent since the amplitude is proportional to the charge of the outgoing ω meson. As discussed in Ref. [16], the π^0 exchange is dominant in the small t region over other meson exchanges and largely responsible for the large diffractive scattering behavior near the threshold. The Lagrangian for the π^0 exchange model has the following form [16]:

$$L_{\pi NN} = -i g_{\pi NN} \bar{\psi} \gamma_5 (\boldsymbol{\tau} \cdot \boldsymbol{\pi}) \psi \quad (85)$$

for the πNN coupling vertex, and

$$L_{\omega \pi^0 \gamma} = e_N \frac{g_{\omega \pi \gamma}}{M_\omega} \epsilon_{\alpha \beta \gamma \delta} \partial^\alpha A^\beta \partial^\gamma \omega^\delta \pi^0 \quad (86)$$

for the $\omega \pi \gamma$ coupling vertex, where the ω^δ and π^0 represent the ω and π^0 fields, the A^β denotes the electromagnetic field, and $\epsilon_{\alpha \beta \gamma \delta}$ is the Levi-Civita tensor, and M_ω is the mass of ω meson. The $g_{\pi NN}$ and $g_{\omega \pi \gamma}$ in Eqs. (85) and (86) denote the coupling constants at the two vertices, respectively. Therefore, the transition amplitudes of t-channel π^0 exchange have the following expression:

$$M_T^t(\pi^0) = \frac{e_N g_{\pi NN} g_{\omega \pi \gamma}}{2 M_\omega (t - m_\pi^2)} \{ \boldsymbol{\omega} \cdot \boldsymbol{\epsilon} \cdot (\mathbf{q} \times \boldsymbol{\epsilon}_v) + \omega_m \mathbf{k} \cdot (\boldsymbol{\epsilon} \times \boldsymbol{\epsilon}_v) \} \boldsymbol{\sigma} \cdot \mathbf{A} e^{-(\mathbf{q}-\mathbf{k})^2/6\alpha_\pi^2} \quad (87)$$

for the transverse transition, and

$$M_L^t(\pi^0) = -\frac{e_N g_{\pi NN} g_{\omega \pi \gamma}}{2 M_\omega (t - m_\pi^2)} \frac{M_\omega}{|\mathbf{q}|} (\boldsymbol{\epsilon} \times \mathbf{k}) \cdot \mathbf{q} \boldsymbol{\sigma} \cdot \mathbf{A} e^{-(\mathbf{q}-\mathbf{k})^2/6\alpha_\pi^2} \quad (88)$$

for the longitudinal transition, where ω in the transition amplitudes denotes the energy of the photon with momentum \mathbf{k} , and $\mathbf{A} = -[\mathbf{q}/(E_f + M_N) + \mathbf{k}/(E_i + M_N)]$, and $t = (q - k)^2 = M_\omega^2 - 2k \cdot q$. The factor $e^{-(\mathbf{q}-\mathbf{k})^2/6\alpha_\pi^2}$ in Eqs. (87) and (88) is the form factor for both πNN and $\omega \gamma \pi$ vertices, if we assume that the wave functions for nucleon, ω and π have a Gaussian form. The constant α_π in this form factor is treated as a parameter. The coupling constants $g_{\pi NN}$ and $g_{\omega \pi \gamma}$ have the values as used in [16]. Therefore,

$$\begin{aligned} \frac{g_{\pi NN}^2}{4\pi} &= 14, \\ g_{\omega \pi \gamma}^2 &= 3.315. \end{aligned} \quad (89)$$

Note that the values of $g_{\pi NN}$ and $g_{\omega \pi \gamma}$ were fixed by separate experiments and, therefore, are not free parameters in Ref. [16]. Qualitatively, we would expect that α_π be smaller than the parameter $\alpha = 410$ MeV, since it represents the combined form factors for both πNN and $\omega \pi \gamma$ vertices while the parameter α only corresponds to the form factor for the πNN or ωNN vertex alone. Following the same procedure as in Sec. II, the explicit expressions for the operators in

TABLE VII. The spatial integrals in the harmonic oscillator basis.

Multiplet	Expression
$[70, 1^-]_1$	$A = \frac{3a}{2m_q \sqrt{3}} \alpha \exp\left(-\frac{\mathbf{q}^2}{6\alpha^2}\right)$ $B = \frac{b'}{m_q} \sqrt{\frac{3}{2}} \frac{\mathbf{q}^2}{\alpha} \exp\left(-\frac{\mathbf{q}^2}{6\alpha^2}\right)$ $S = \frac{\sqrt{3}\mu a}{\alpha} \exp\left(-\frac{\mathbf{q}^2}{6\alpha^2}\right)$
$[56, 2^+]_2$	$A = -\frac{a}{2\sqrt{2}m_q} \mathbf{q} \exp\left(-\frac{\mathbf{q}^2}{6\alpha^2}\right)$ $B = -\frac{b'}{2\sqrt{3}m_q} \mathbf{q} \left(\frac{\mathbf{q}}{\alpha}\right)^2 \exp\left(-\frac{\mathbf{q}^2}{6\alpha^2}\right)$ $S = -\frac{\mu a}{\sqrt{6} \mathbf{q} } \left(\frac{\mathbf{q}}{\alpha}\right)^2 \exp\left(-\frac{\mathbf{q}^2}{6\alpha^2}\right)$
$[56, 0^+]_2$	$B = \frac{b'}{2\sqrt{3}m_q} \mathbf{q} \left(\frac{\mathbf{q}}{\alpha}\right)^2 \exp\left(-\frac{\mathbf{q}^2}{6\alpha^2}\right)$ $S = \frac{\mu a}{\sqrt{6} \mathbf{q} } \left(\frac{\mathbf{q}}{\alpha}\right)^2 \exp\left(-\frac{\mathbf{q}^2}{6\alpha^2}\right)$
$[56, 0^+]_0$	$B = \frac{3b'}{\sqrt{2}m_q} \mathbf{q} \exp\left(-\frac{\mathbf{q}^2}{6\alpha^2}\right)$ $S = \frac{3\mu a}{ \mathbf{q} } \exp\left(-\frac{\mathbf{q}^2}{6\alpha^2}\right)$
$[70, 0^+]_2$	$B = -\frac{b'}{2\sqrt{6}m_q} \mathbf{q} \left(\frac{\mathbf{q}}{\alpha}\right)^2 \exp\left(-\frac{\mathbf{q}^2}{6\alpha^2}\right)$ $S = -\frac{\mu a}{2\sqrt{3} \mathbf{q} } \left(\frac{\mathbf{q}}{\alpha}\right)^2 \exp\left(-\frac{\mathbf{q}^2}{6\alpha^2}\right)$
$[70, 2^+]_2$	$A = \frac{a}{2\sqrt{2}m_q} \mathbf{q} \exp\left(-\frac{\mathbf{q}^2}{6\alpha^2}\right)$ $B = \frac{b'}{2\sqrt{3}m_q} \mathbf{q} \left(\frac{\mathbf{q}}{\alpha}\right)^2 \exp\left(-\frac{\mathbf{q}^2}{6\alpha^2}\right)$ $S = \frac{\mu a}{\sqrt{6} \mathbf{q} } \left(\frac{\mathbf{q}}{\alpha}\right)^2 \exp\left(-\frac{\mathbf{q}^2}{6\alpha^2}\right)$

terms of the helicity amplitudes can be obtained. They are listed in Tables II and III for the transverse and longitudinal amplitudes, respectively.

As shown in Table IV, the Moorhouse selection rule [27] has eliminated the states belonging to $[70, 1^-]_1$ and $[70, 2^+]_2$ representations with symmetric spin structure from contributing to the ω photoproduction on the proton target so that the s-channel states $S_{11}(1650), D_{13}(1700), D_{15}(1650)$ are not present in our numerical evaluations. Of course, configuration mixing will lead to additional contributions from these resonances which, however, cannot be determined at present due to the poor quality of data. Only the resonances $P_{13}(1900)$ and $F_{15}(2000)$, at present classified as 2-star resonances in the 1996 Particle Data Group (PDG) listings,

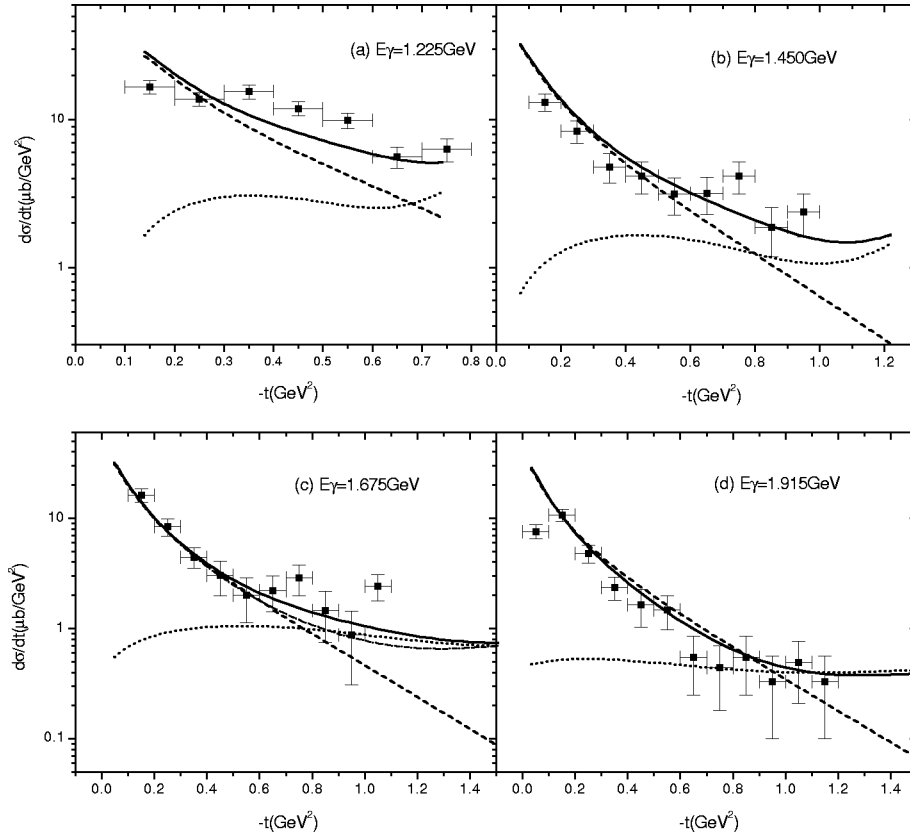


FIG. 1. The differential cross sections (solid curves) for $\gamma p \rightarrow \omega p$ at $E_\gamma = 1.225, 1.45, 1.675,$ and 1.915 GeV. The data come from Ref. [3]. The π^0 exchanges are shown by the dashed curves and the contributions from s- and u-channel exclusively are shown by the dotted curves. In (c), the dot-dashed curve represents the differential cross section without contributions from the resonance $F_{15}(2000)$.

have masses above the ω decay threshold, and therefore have branching ratio into the ωN channel. We have not performed a rigorous numerical fit to the available data because of the poor quality of the data. However, the numerical results have shown that the resonance $F_{15}(2000)$ plays a very important role in ω photoproduction.

Figure 1 shows our calculations for the differential cross section at the average photon energies of $E_\gamma = 1.225, 1.45, 1.675,$ and 1.915 GeV, in comparison with the data [3]. The results for the t-channel π^0 exchange and contributions from only the s- and u-channel processes are also shown separately. We find that the remaining parameters in our model are

$$\begin{aligned} a &= -1.7 \\ b' &= 2.5 \\ \alpha_\pi &= 300 \text{ MeV}, \end{aligned} \quad (90)$$

in order to give a good overall agreement with the data, particularly in the large t region. Our results with the π^0 exchange are consistent with the findings of Ref. [16] though the form factor in our calculation is different. Figure 1 clearly demonstrates that the t-channel π^0 exchange is dominant in the small t region, while the s- and u-channel resonance contributions become more important as the momentum transfer t increases. To test the sensitivity of s-channel resonances to the differential cross section, the differential cross section without the contribution from the resonance $F_{15}(2000)$ at 1.675 GeV [near the threshold of $F_{15}(2000)$] is

presented in Fig. 1(c) as well. The results indicate that the differential cross section data alone are not sufficient to determine the presence of this resonance considering the theoretical and experimental uncertainties. Since our numerical calculation shows that the resonance couplings of the $F_{15}(2000)$ are larger than those of other resonances in this mass region, the sensitivity of the differential cross section to other resonances around 2 GeV is even smaller.

In contrast to the differential cross section, the polarization observables show a much more dramatic dependence on the presence of the s-channel resonances. We present results of four single polarizations at 1.7 GeV in Fig. 2. The absence of the resonance $F_{15}(2000)$ leads to a sign change in the target polarization, and the variations in the recoil as well as the meson polarization observable are very significant as well. The absence of the resonance $P_{13}(1900)$, also shown in Fig. 2, leads to very significant changes in the recoil polarization. Although we do not expect our numerical results to give a quantitative prediction of polarization observables at the present stage, since the calculations are limited to the $SU(6) \otimes O(3)$ symmetry limit that should be broken in a more realistic quark model wave function, our results clearly suggest that the polarization observables may be the best place to determine s-channel resonance properties.

Our results for the total cross section are shown in Fig. 3, in which the contributions from the s- and u-channel resonances alone are compared to the full calculation. Our results indicate an increasing discrepancy between theory and the data [3,5,28] with increasing energy E_γ . This discrepancy comes mainly from the small angle region where the π^0

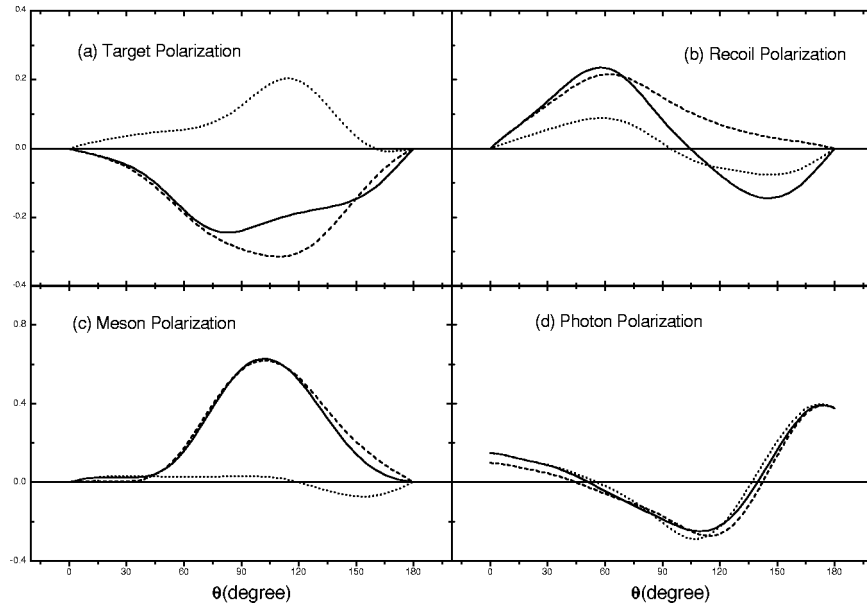


FIG. 2. The four single-spin polarization observables in $\gamma p \rightarrow \omega p$ are given by the solid curves at $E_\gamma = 1.7$ GeV. The dotted curves correspond to the asymmetries without the resonance $F_{15}(2000)$, while the dashed curves correspond to those without the resonance $P_{13}(1900)$.

exchange alone is not sufficient to describe the diffractive behavior at higher energies. One might expect that Pomeron exchange [10,29] plays a more important role in the higher energy region. However, Fig. 1 shows that our results for the differential cross section at the large angle region are in good agreement with the data, and it suggests that contributions from the s- and u-channel resonances which are the main focus of our study, give an appropriate description of the reaction mechanism.

It is interesting to note that the small bump around 1.7 GeV in the total cross section comes from the contributions of the resonance $F_{15}(2000)$. As discussed above, our calculations find that the resonance $F_{15}(2000)$ has a strong coupling to the ωN channel. Thus, this resonance is perhaps the best candidate whose existence as a “missing” resonance can be established through ω photoproduction.

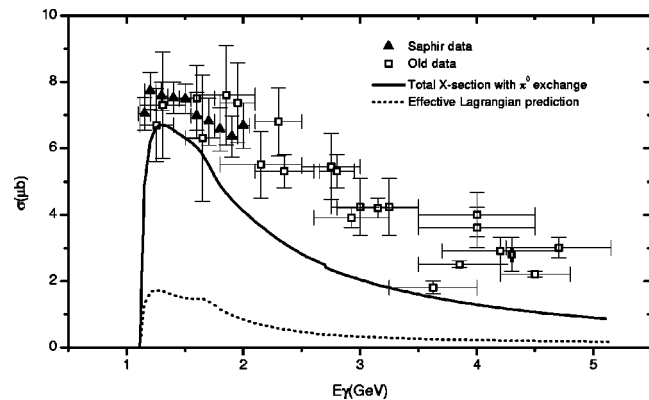


FIG. 3. The total cross section of $\gamma p \rightarrow \omega p$ is fitted by the solid curve with π^0 exchange taken into account. The dotted curve describes the pure contributions from s- and u-channel. The data are from Ref. [3] (triangle), [5], and other experiments [28] (square).

B. ρ^0 photoproduction

ρ^0 meson photoproduction has some similar features as ω photoproduction. The most significant one is that it also has strong-forward-peaking diffractive behavior in the differential cross section. The t-channel vector meson exchange is proportional to the meson charge in Eq. (14), therefore has no contributions to the transition amplitudes. However, since the ρ meson is an isovector, its photoproduction has also shown some different characters from ω photoproduction. There are more s-channel resonances, such as the Δ resonances, which will contribute to the ρ^0 productions due to the isospin couplings.

From the Lagrangian introduced in our quark model approach, the amplitudes from s- and u-channel are not sufficient to reproduce the diffractive behavior in the small t region. Following what we have discussed at the beginning of this section, it is reasonable to include an additional t-channel meson exchange term in the transition amplitude [13]. As Friman and Soyeur [16] have discussed in their work, the σ meson plays a dominant role over other t-channel processes in the ρ^0 photoproduction. As a phenomenological approach, σ exchange is included to give the small t diffractive behavior which can be understood as the still sizable contribution from the Pomeron exchange from high energies down to the threshold [14,15]. In terms of Regge phenomenology, it corresponds to the nontrivial background integral of the Regge trajectory expansion [13] which contributes to the diffractive behavior at small t region. However, we have to mention that, only if the resonance contributions have been taken into account consistently, could the proper large t behavior be described. The following are the transverse and longitudinal transition amplitudes of σ exchange:

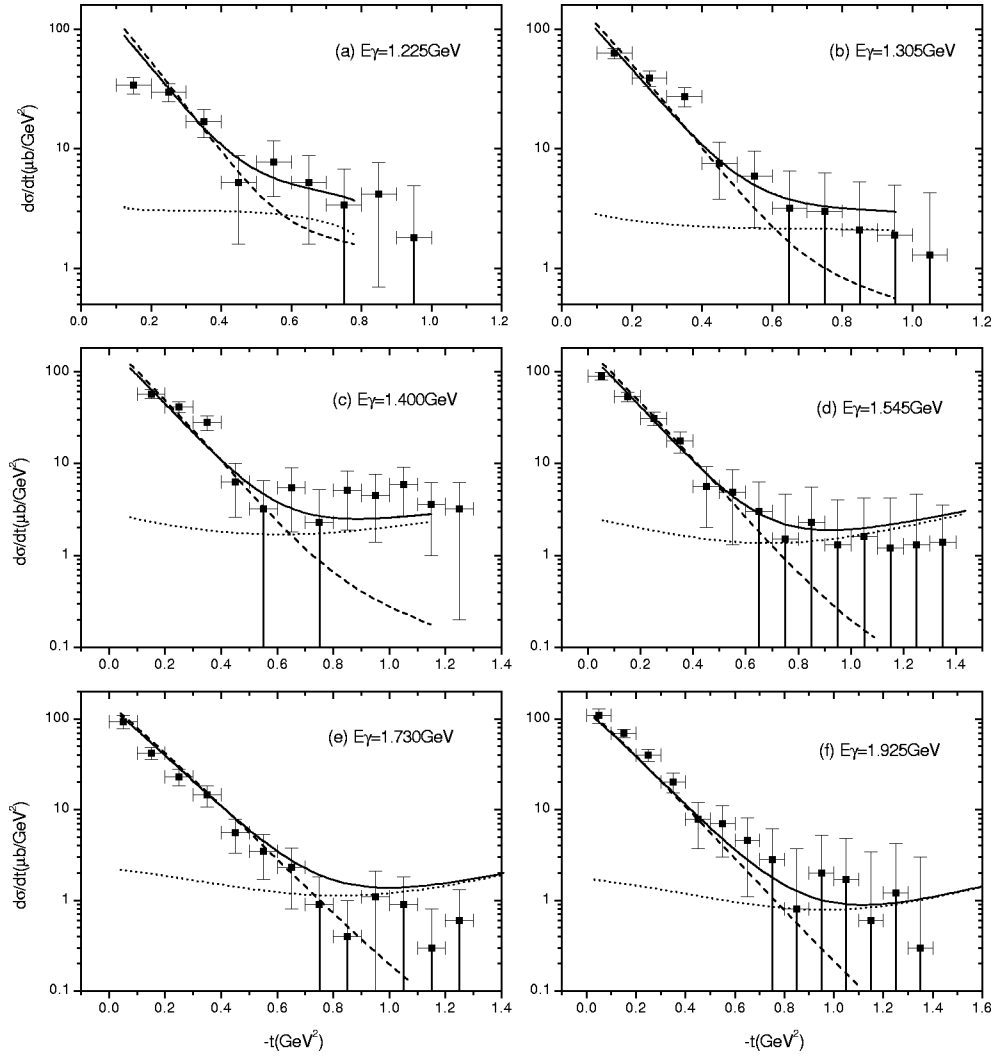


FIG. 4. The differential cross sections (solid curves) for $\gamma p \rightarrow \rho^0 p$ at $E_\gamma = 1.225, 1.305, 1.400, 1.545, 1.730,$ and 1.925 GeV. The data come from Ref. [3]. The σ exchanges are shown by the dashed curves and the contributions from s- and u-channel exclusively are shown by the dotted curves.

$$M_T^i(\sigma) = \frac{ie_{NN}g_{\sigma NN}g_{\rho^0\sigma\gamma}}{M_\rho(M_\rho^2 - 2q \cdot k - M_\sigma^2)} \{-\omega\omega_m \boldsymbol{\epsilon} \cdot \boldsymbol{\epsilon}_v + \mathbf{k} \cdot \mathbf{q} \boldsymbol{\epsilon} \cdot \boldsymbol{\epsilon}_v - \mathbf{q} \cdot \mathbf{k} \boldsymbol{\epsilon} \cdot \boldsymbol{\epsilon}_v\} e^{-(\mathbf{q}-\mathbf{k})^2/6\alpha_\sigma^2}, \quad (91)$$

$$\frac{g_{\sigma NN}^2}{4\pi} = 8,$$

$$g_{\rho^0\sigma\gamma}^2 = 7.341. \quad (93)$$

$$M_L^i(\sigma) = \frac{ie_{NN}g_{\sigma NN}g_{\rho^0\sigma\gamma}}{M_\rho^2(M_\rho^2 - 2q \cdot k - M_\sigma^2)} \omega |\mathbf{q}| \mathbf{q} \cdot \boldsymbol{\epsilon} e^{-(\mathbf{q}-\mathbf{k})^2/6\alpha_\sigma^2}, \quad (92)$$

where $e^{-(\mathbf{q}-\mathbf{k})^2/6\alpha_\sigma^2}$ is the form factor for t-channel σ exchange. α_σ is treated as the parameter. $g_{\sigma NN}$ and $g_{\rho^0\sigma\gamma}$ are the coupling constants of the vertex σNN and $\rho^0\sigma\gamma$, respectively, which are determined by the experimental analysis. As a phenomenological freedom, the mass of σ meson M_σ has the same values as in [16], $M_\sigma = 500$ GeV. $g_{\sigma NN}$ and $g_{\rho^0\sigma\gamma}$ have the following values:

Numerical investigation indicates that π^0 exchange contribution in ρ^0 photoproduction is so small that it can be neglected in the first order approximation. With the same values for parameter a and b' , we fit the differential cross sections, total cross section, and the single spin polarizations in $\gamma p \rightarrow \rho^0 p$. For $n \leq 2$, there are 27 resonances given by the quark model. However, the Moorhouse selection rule will eliminate those belonging to the representation $[\mathbf{70}, 1^-]_1$, $[\mathbf{70}, 0^+]_2$, and $[\mathbf{70}, 2^+]_2$, in which there are $S_{11}(1650)$, $D_{13}(1700)$, and $D_{15}(1675)$ belonging to $[\mathbf{70}, 1^-]_1$, but those belonging to $[\mathbf{70}, 0^+]_2$ and $[\mathbf{70}, 2^+]_2$ have not been determined very well in experiments.

The experimental data from [3] have been reproduced in our model at $E_\gamma = 1.225, 1.305, 1.4, 1.545, 1.730, 1.925$ GeV

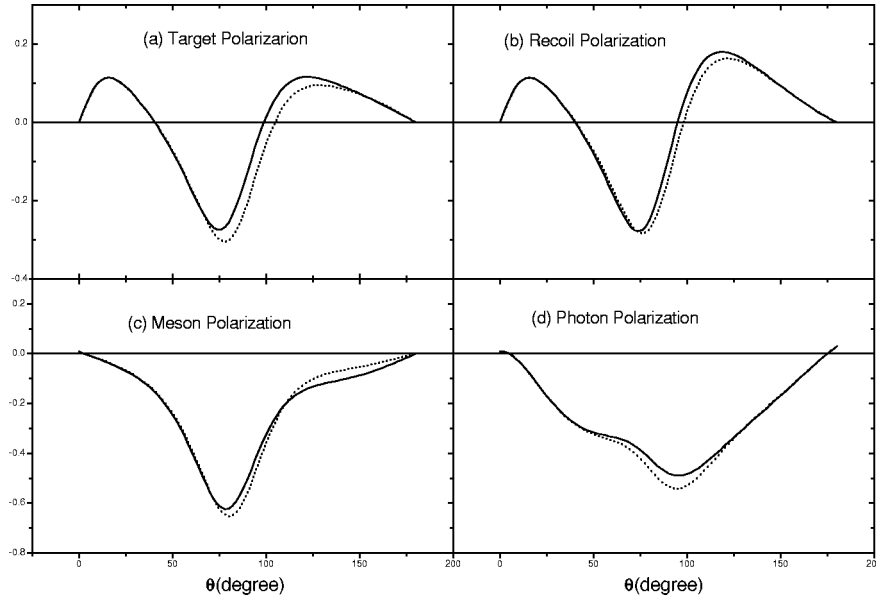


FIG. 5. The four single-spin polarization observables in $\gamma p \rightarrow \omega p$ are given by the solid curves at $E_\gamma = 1.7$ GeV. The dotted curves correspond to the asymmetries without the resonance $F_{15}(2000)$.

for the differential cross sections. We find that the same set of parameters in the ω could also be used to describe the ρ productions as well. The additional parameter α_σ is found to be

$$\alpha_\sigma = 250 \text{ MeV}. \quad (94)$$

The fact that both ω and ρ^0 production can be described by the same set of the parameters is by no means trivial. It shows the advantage of the introduction of the quark degrees of freedom so that the ω and ρ can be described by a unified framework, moreover, the isospin mixing between ω and ρ is small and they have very similar masses. Although the σ exchange dominates in the small t region, s- and u-channel contributions play obviously important roles in the large t region. In fact, it is the s- and u-channel contributions that result in the backward peaking behavior which is similar to the Compton scattering phenomenon [30]. In Fig. 4, the individual results from σ exchange and s- and u-channel are presented as well. It shows that the cross sections are mainly from the diffractive process. Moreover, since the number of contributing resonances is large, the contribution effects from individual resonance are not significant. That is to say, it is quite impossible to derive the resonance informations from the differential cross sections.

The polarization results are provided in Fig. 5. Much attention has been paid to the ‘‘missing resonance’’ $F_{15}(2000)$. It shows that the polarization observables are quite sensitive to the presence of this state, especially in the recoil polarization and meson polarization. Double spin polarization investigations are in progress in our framework and they should be more sensitive to the resonances.

In Fig. 6 all available data [3,5,28] for $\gamma p \rightarrow \rho^0 p$ are present. With the same set of parameters, the theoretical result gives a good description of the experimental data. In Fig. 6 the dotted line denotes the contributions from s- and u-channel which shows that the cross section of producing ρ^0 through resonance channel is quite small in contrast with that

through diffractive process. This also explains why the effects of an individual resonance is not significant in the differential cross sections.

C. ρ^\pm photoproduction

In the charge meson productions, $\gamma n \rightarrow \rho^- p$ and $\gamma p \rightarrow \rho^+ n$, the three channels s-, u-, and t- have contributions to the transition amplitudes. The charge exchange process has eliminated contributions from such diffractive behaviors as in the ω and ρ^0 photoproduction while the t-channel charged vector meson exchange and the Seagull term will account for the small forward peaking shapes of the differential cross sections, and this is also required by the duality hypothesis when we have taken the contributions from all the s- and u-channel processes into account. Therefore, charged meson production provides an important test of this approach, as every term in these two reactions is generated by the effective Lagrangian, and there are no additional free parameters.

In $\gamma p \rightarrow \rho^+ n$, for the Moorhouse selection rule at the photon interaction vertex, those resonances belonging to

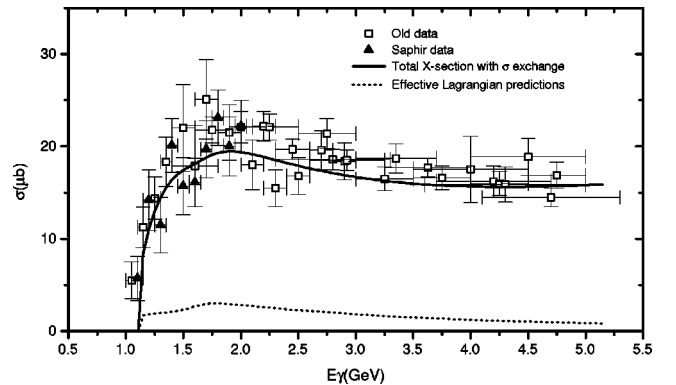


FIG. 6. The total cross section of $\gamma p \rightarrow \rho^0 p$ is fitted by the solid curve with σ exchange taken into account. The dotted curve describes the pure contributions from s- and u-channel. The data are from Ref. [3] (triangle), [5], and other experiments [28] (square).

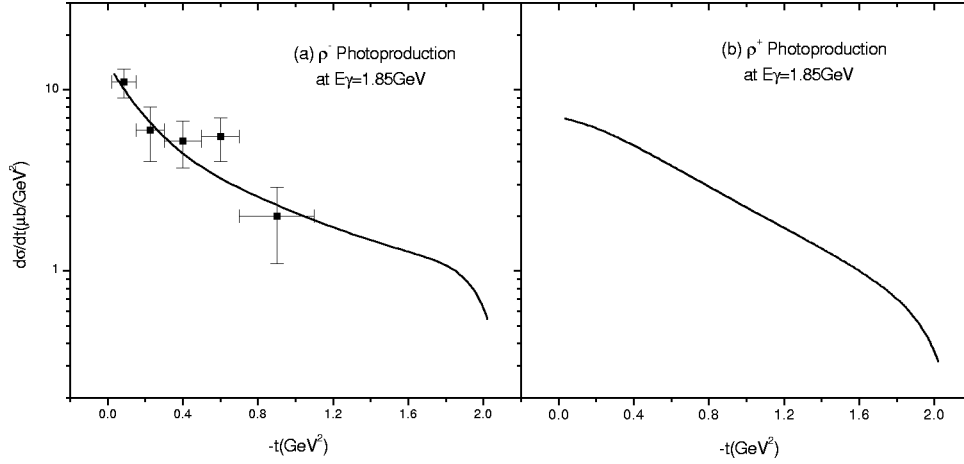


FIG. 7. The differential cross sections for (a) $\gamma n \rightarrow \rho^- p$, and (b) $\gamma p \rightarrow \rho^+ n$ at $E_\gamma = 1.85$ GeV. The data in (a) come from Ref. [6].

$[70, 1^-]_1$, $[70, 0^+]_2$, and $[70, 2^+]_2$ are eliminated from contributing to the amplitudes. But in $\gamma n \rightarrow \rho^- p$, without the constraint from Moorhouse selection rule, more resonances have contributions to the amplitudes.

As we have shown in the ω and ρ^0 photoproduction, the same set of parameters a and b' gives an overall agreement with the available data; the challenge is whether we can reproduce the data [6] in the ρ^\pm channels with the same parameters, because they possess the same isospin symmetry. This should be one crucial test for the model. As expected, the data in the reaction $\gamma n \rightarrow \rho^- p$ are in very good agreement with the quark model predictions, indicating that the quark model wave functions appear to provide the correct relative strengths and phases among the terms in the s -, u - and t -channels. In Fig. 7(a), the experimental data for $\gamma n \rightarrow \rho^- p$ from Ref. [6] are presented at $E_\gamma = 1.85$ GeV, which is the average of the measurement realm. In Fig. 7(b), we present the prediction of the differential cross section in $\gamma p \rightarrow \rho^+ n$, and it shows a similar behavior as in $\gamma n \rightarrow \rho^- p$.

In Fig. 8, the total cross sections for ρ^\pm [6] are presented. In Fig. 8(a), the cross section of ρ^- photoproduction with $0 < |t| < 1.1$ GeV² is well reproduced, along which the total cross section is also consistent with the experimental estimation [7]. The prediction of the total cross section of ρ^+ pho-

toproduction is given in Fig. 8(b).

While the shapes and magnitudes of the differential cross sections are well reproduced within our approach we find little sensitivity to individual resonances. For example, in the energy region of $E_\gamma \sim 1.7$ GeV, removing the $F_{15}(2000)$ state—one of the “missing” candidates—changes the cross section very little, indicating the differential cross section may not be the ideal experimental observable to study the structure of the baryon resonances. In contrast to the cross sections, the polarization observables show a more dramatic dependence on the presence of the s -channel resonances. To illustrate their effects, as an example, the target polarizations for ρ^- and ρ^+ production with and without the contribution from the $F_{15}(2000)$ resonance are shown in Fig. 9. We do not expect the quark model in the $SU(6) \otimes O(3)$ limit to provide a good description of these observables. However, it demonstrates the sensitivity of these observables to the presence of s -channel resonances. This shows that polarization observables are essential in analyzing the role of s -channel resonances.

D. The ϕ photoproduction

Because the isospin of the ϕ is the same as that of the ω , the formalism for the s - and u -channel contributions to the ϕ

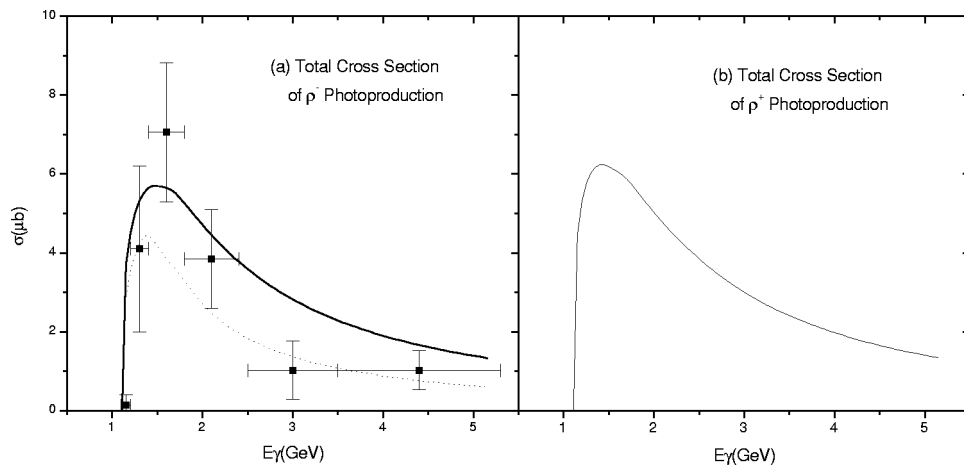


FIG. 8. The total cross section for (a) $\gamma n \rightarrow \rho^- p$, and (b) $\gamma p \rightarrow \rho^+ n$. The dotted line in (a) represents the cross section for $|t| \leq 1.1$ GeV². The data in (c) were taken with the restriction $|t| \leq 1.1$ GeV² given by Ref. [6].

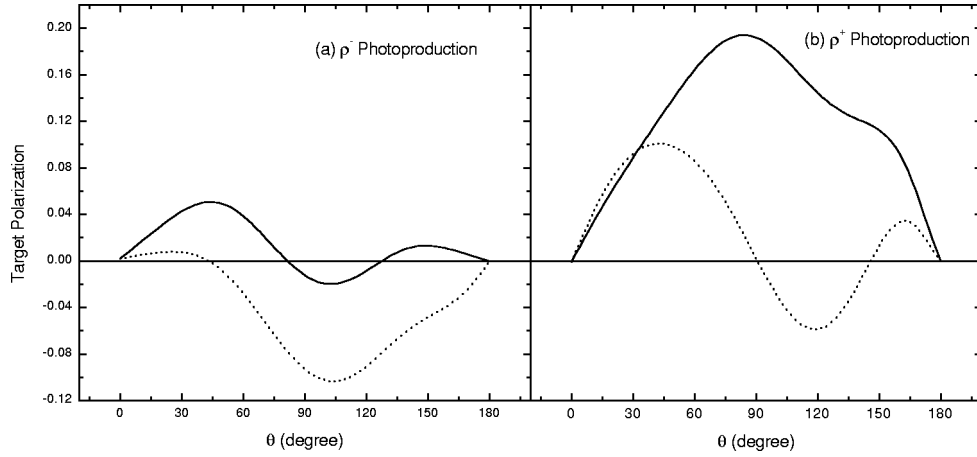


FIG. 9. The target polarizations for (a) $\gamma n \rightarrow \rho^- p$, and (b) $\gamma p \rightarrow \rho^+ n$ at $E_\gamma = 1.7$ GeV. The dotted lines show the results without the contribution from the $F_{15}(2000)$.

productions should be the same as that of the ω productions except the different threshold energies. The major difference between the ω and the ϕ productions is the mechanism of generating u (d) and \bar{u} (\bar{d}) quarks for the ω productions and the s and \bar{s} quarks for the ϕ production that are suppressed by the OZI rule. Such a difference will be reflected in the difference of the coupling constants between ω and ϕ productions, of which the coupling constant for the ϕNN vertex is expected to be much smaller than that for the ωNN vertex. Thus, we shall concentrate on the nondiffractive effects generated from the effective Lagrangian in the s- and u-channel reaction. Since we have not included the Pomeron exchange term to give the strong diffractive behavior in the small t region, our results thus could only be regarded as an estimation.

The numerical results with the following two sets of parameters are shown in comparison with the data [8] in Fig. 10. They represent the ϕqq coupling constants in the non-diffractive processes of the ϕ production,

$$\begin{aligned} a &= -0.35, \\ b' &= 0.7, \end{aligned} \tag{95}$$

and

$$\begin{aligned} a &= -0.6, \\ b' &= 1.2. \end{aligned} \tag{96}$$

It should be noted that the same value of α as that in the ω production has been used in the evaluations at present stage. Our results show that the differential cross sections are very sensitive to the parameters a and b' in the large t region, where the Pomeron exchange is expected to be small. Thus, the data in the large t region could provide an important constraint to the ϕNN coupling constants. Moreover, the coupling constants in Eqs. (95) and (96) are indeed significantly smaller than those for the ω photoproductions in Eq. (90). These results are also consistent with those obtained in the QHD approach [18].

V. DISCUSSION AND CONCLUSION

In this paper we have developed the framework and formalism for the description of the vector meson photoproductions in the constituent quark model. Consequently, the application of this approach to the ω and ρ meson photoproduction has produced very encouraging results. The use of an effective Lagrangian allows the gauge invariance to be satisfied straightforwardly.

The advantage of using the quark model approach is that the number of free parameters is greatly reduced in comparison with hadronic models which introduce each resonance as a new independent field with unknown coupling constants. In our approach, only three parameters appear in the $SU(6) \otimes O(3)$ symmetry limit, the coupling constants a and b (or b') which determine the coupling strengths of the vector meson to the quark, and the harmonic oscillator strength α .

With π^0 and σ exchange taken into account, an overall description of the ω , ρ^0 , ρ^+ , and ρ^- photoproduction with the same set of parameters has been obtained in this framework. It shows that intermediate resonance contributions have played important roles in the ω and ρ meson photoproduction especially in large t regions. This shows that our effective Lagrangian approach in the quark model has provided an ideal framework to investigate the reaction mechanism and the underlying quark structure of the baryon resonances. The crucial role played by the polarization observables in determining the s-channel resonance properties is demonstrated. Data on these observables, expected from TJNAF in the near future, should therefore provide new insights into the structure of the resonance $F_{15}(2000)$ as well as other ‘‘missing’’ resonances.

The introduction of t-channel π^0 and σ exchange in the neutral productions can be quantitatively understood in the picture of the Regge phenomenology [13] or the diffraction duality picture of Freund [14] and Harari [15]. In such a picture, the large difference of the cross section between ρ^0 and ρ^\pm is due to such a background amplitude which originates from a sizable contribution of the Pomeron singularity in ρ^0 photoproduction from high energies down to the threshold. Our numerical investigation has really shown the case, therefore, to some extent, suggests that the duality hy-

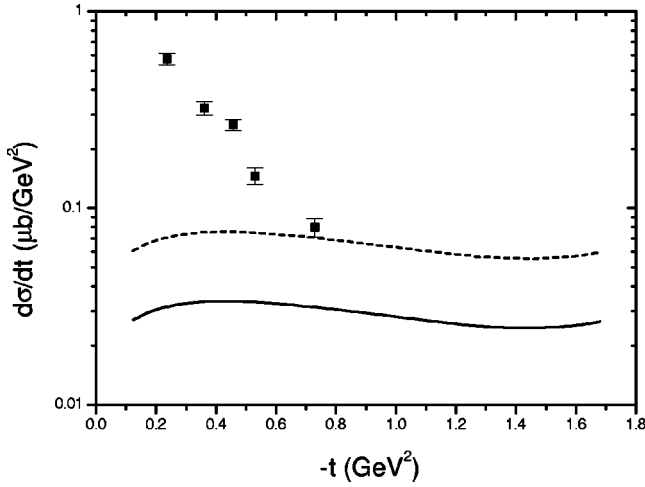


FIG. 10. The nondiffractive contributions from the effective Lagrangian to the differential cross section of the ϕ photoproduction at $E_\gamma=2.0$ GeV. The data come from Ref. [8]. The solid and dashed curve represent the results with parameters of Eqs. (95) and (96), respectively.

pothesis [31] constrains also the vector meson photoproductions.

In the reaction of ϕ photoproduction, the sizable nondiffractive contributions can be phenomenologically interpreted as the s- and u-channel contributions generated from the effective Lagrangian. Further studies that include the Pomeron exchange in this approach will be pursued later.

One significant approximation inherent in the presented approach is the treatment of the vector mesons as point particles; thus, the effects due to the finite size of the vector

mesons that were important in the 3P_0 model are neglected here. A possible way that may partly compensate this problem is to adjust the parameter α^2 , the harmonic oscillator strength. In general, the question of how to include the finite size of vector mesons while maintaining the gauge invariance is very complicated and has not yet been resolved. Moreover, as configuration mixing effects for the resonances in the second and third resonance region are known to be very important, more precise quantitative agreement with the data cannot be derived from the current form. But such effects could be investigated in our approach by inserting a mixing parameter C_R in front of the transition amplitudes for the s-channel resonances, as has been investigated in Ref. [26].

The fact that the ω and ρ productions can be described by the same set of parameters shows the successes of the quark model approach. Thus, the model presented here could provide a systematic method to investigate the resonance behavior in the vector meson photoproduction for the first time, which will help us to identify the ‘‘missing resonances.’’

ACKNOWLEDGMENTS

The authors acknowledge useful discussions with B. Saghai, F. Tabakin, and P. Cole. Helpful discussions with F. J. Klein regarding the data are acknowledged gratefully. Zhenping Li acknowledges the hospitality of the Saclay Nuclear Physics Laboratory. Q. Zhao acknowledges helpful discussions with Yang Ze-sen and Hongan Peng. This work was supported in part by the Chinese Education Commission and Peking University, and U.S.-DOE Grant No. DE-FG02-95-ER40907.

APPENDIX

The matrix element for the nucleon pole term of transverse excitations in the s-channel is

$$M_N^s(T) = -\frac{M_N e^{-(q^2+k^2)/6\alpha^2}}{P_N \cdot k} \left\{ g_v^t \frac{\omega a e_N}{E_f + M_f} \boldsymbol{\epsilon}_v \cdot \boldsymbol{\epsilon} - g_A \mu_N \frac{b'}{2m_q} [(\boldsymbol{\epsilon}_v \times \mathbf{q}) \cdot (\boldsymbol{\epsilon} \times \mathbf{k}) + i \boldsymbol{\sigma} \cdot (\boldsymbol{\epsilon}_v \times \mathbf{q}) \times (\boldsymbol{\epsilon} \times \mathbf{k})] \right\}, \quad (97)$$

while the one for the u-channel is

$$M_N^u(T) = -\frac{M_f e^{-(q^2+k^2)/6\alpha^2}}{P_f \cdot k} \left\{ g_v^t \frac{\omega a e_f}{E_N + M_N} \boldsymbol{\epsilon} \cdot \boldsymbol{\epsilon}_v + g_A \mu_f \frac{b'}{2m_q} [(\boldsymbol{\epsilon} \times \mathbf{k}) \cdot (\boldsymbol{\epsilon}_v \times \mathbf{q}) + i \boldsymbol{\sigma} \cdot ((\boldsymbol{\epsilon} \times \mathbf{k}) \times (\boldsymbol{\epsilon}_v \times \mathbf{q}))] \right\} \\ + \frac{e_f e^{-(q^2+k^2)/6\alpha^2}}{P_f \cdot k} \left\{ \frac{-g_v^t a}{E_N + M_N} \mathbf{q} \cdot \boldsymbol{\epsilon} \mathbf{k} \cdot \boldsymbol{\epsilon}_v + i g_A \frac{b'}{2m_q} \boldsymbol{\sigma} \cdot (\boldsymbol{\epsilon}_v \times \mathbf{q}) \mathbf{q} \cdot \boldsymbol{\epsilon} \right\}. \quad (98)$$

The matrix element for the nucleon pole term of the longitudinal excitations in the s-channel is

$$M_N^s(L) = -g_v^t \frac{i \mu a (w + M_N)}{|\mathbf{q}|} \frac{1}{2P_N \cdot k} \mu_N \boldsymbol{\sigma} \cdot (\boldsymbol{\epsilon} \times \mathbf{k}) e^{-(q^2+k^2)/6\alpha^2}, \quad (99)$$

while the one for the u-channel is

$$M_N^u(L) = g_v^t \frac{\mu a}{|\mathbf{q}|} \frac{1}{P_f \cdot k} \left\{ -e_f \mathbf{q} \cdot \boldsymbol{\epsilon} + i \mu_f \frac{(w + M_f)}{2w} \boldsymbol{\sigma} \cdot (\boldsymbol{\epsilon} \times \mathbf{k}) \right\} e^{-(q^2+k^2)/6\alpha^2}, \quad (100)$$

where $w = E_i + \omega = E_f + \omega_m$ is the c.m. energy and the g -factor g_v^t has been given in Eq. (32).

The t-channel matrix element for the transverse transition is

$$\begin{aligned}
 M^t(T) = & -\frac{ae_m}{q \cdot k} \left\{ -g_v^t \left[\omega_m + \left(\frac{\mathbf{q}}{E_f + M_f} + \frac{\mathbf{k}}{E_N + M_N} \right) \cdot \mathbf{q} \right] \boldsymbol{\epsilon} \cdot \boldsymbol{\epsilon}_v + g_A \frac{i}{2m_q} \boldsymbol{\sigma} \cdot (\mathbf{k} \times \mathbf{q}) \boldsymbol{\epsilon} \cdot \boldsymbol{\epsilon}_v \right. \\
 & - g_v^t \left(\frac{1}{E_f + M_f} + \frac{1}{E_N + M_N} \right) \mathbf{q} \cdot \boldsymbol{\epsilon} \mathbf{k} \cdot \boldsymbol{\epsilon}_v + g_A \frac{i}{2m_q} \boldsymbol{\sigma} \cdot ((\mathbf{k} - \mathbf{q}) \times \boldsymbol{\epsilon}_v) \mathbf{q} \cdot \boldsymbol{\epsilon} \\
 & \left. + g_A \frac{i}{2m_q} \boldsymbol{\sigma} \cdot ((\mathbf{k} - \mathbf{q}) \times \boldsymbol{\epsilon}) \mathbf{k} \cdot \boldsymbol{\epsilon}_v \right\} e^{-(\mathbf{k} - \mathbf{q})^2 / 6\alpha^2}, \tag{101}
 \end{aligned}$$

and for the longitudinal transition it is

$$M^t(L) = -\frac{\mu}{|\mathbf{q}|} \frac{ae_m}{q \cdot k} \left\{ g_v^t \left(1 - \frac{\omega}{E_f + M_f} \right) \mathbf{q} \cdot \boldsymbol{\epsilon} + g_A \frac{i\omega}{2m_q} \boldsymbol{\sigma} \cdot ((\mathbf{k} - \mathbf{q}) \times \boldsymbol{\epsilon}) \right\} e^{-(\mathbf{k} - \mathbf{q})^2 / 6\alpha^2}. \tag{102}$$

[1] N. Isgur and G. Karl, Phys. Lett. **72B**, 109 (1977); Phys. Rev. D **23**, 817 (1981); R. Koniuk and N. Isgur, *ibid.* **21**, 1868 (1980).

[2] S. Capstick and W. Roberts, Phys. Rev. D **49**, 4570 (1994).

[3] F. J. Klein, to appear in the Proceedings of the GW/TJNAF Workshop on N^* Physics, Washington, D.C., 1997; F. J. Klein, Ph.D. thesis, University of Bonn, 1996.

[4] TJNAF experimental proposal E94-109 (P. Cole and R. Whitney, co-spokesmen); E91-024 (V. Burkert, H. Funsten, M. Manley, and B. Mecking, co-spokesmen).

[5] ABBHHM Collaboration, Phys. Rev. **175**, 1669 (1968).

[6] P. Benz *et al.*, Nucl. Phys. **B79**, 10 (1974).

[7] H. G. Hilpert *et al.*, Nucl. Phys. **B21**, 93 (1970).

[8] H. J. Besch *et al.*, Nucl. Phys. **B70**, 257 (1974).

[9] T. H. Bauer, R. D. Spital, D. R. Yennie, and F. M. Pipkin, Rev. Mod. Phys. **50**, 261 (1978).

[10] M. Pichowsky, "Nonperturbative Quark Dynamics in diffractive processe," Ph.D. dissertation, The University Of Pittsburgh, 1996, and references therein.

[11] Zhenping Li *et al.*, Phys. Rev. C **56**, 1099 (1997).

[12] A. Le Yaouanc *et al.*, *Hadron Transitions in the Quark Model* (Gordon and Breach, New York, 1988)

[13] P. D. B. Collins, *An Introduction to Regge Theory and High-energy Physics* (Cambridge University Press, Cambridge, 1997).

[14] P. G. O. Freund, Phys. Rev. Lett. **20**, 235 (1968).

[15] H. Harari, Phys. Rev. Lett. **20**, 1395 (1968).

[16] B. Friman and M. Soyeur, Nucl. Phys. **A100**, 477 (1996).

[17] J. Reifenrother *et al.*, The ASTERIX Collaboration, Phys. Lett. B **267**, 299 (1991); M. A. Faessler *et al.*, The Crystal Barrel Collaboration, Phys. At. Nucl. **57**, 1693 (1994); V. G. Ableev *et al.*, The OBELIX Collaboration, *ibid.* **57**, 1716 (1994); Phys. Lett. B **334**, 237 (1994).

[18] R. A. Williams, Phys. Rev. C **57**, 223 (1998).

[19] M. Pichowsky, Ç. Şavklı, and F. Tabakin, Phys. Rev. C **53**, 593 (1996).

[20] K. Schilling, P. Seyboth, and G. Wolf, Nucl. Phys. **B15**, 397 (1970); **B18**, 332(E) (1970).

[21] J. Ballam *et al.*, Phys. Rev. D **5**, 545 (1972).

[22] Zhenping Li, Phys. Rev. D **48**, 3070 (1993).

[23] J. M. Blatt and V. F. Weisskopf, *Theoretical Nuclear Physics* (Wiley, New York, 1952), p. 361.

[24] Zhenping Li, "Photo- and Electroproduction of Baryon Resonances in A Potential Quark Mode," Ph.D. dissertation, The University of Tennessee, 1991.

[25] Ç. Şavklı, F. Tabakin, and S. N. Yang, Phys. Rev. C **53**, 1132 (1996).

[26] Zhenping Li, Phys. Rev. D **52**, 4961 (1995).

[27] R. G. Moorhouse, Phys. Rev. Lett. **16**, 772 (1966).

[28] H. R. Crouch *et al.*, Phys. Rev. **155**, 1468 (1967); Y. Eisenberg *et al.*, Phys. Rev. D **5**, 15 (1972); Y. Eisenberg *et al.*, Phys. Rev. Lett. **22**, 669 (1969); D. P. Barber *et al.*, Z. Phys. C **26**, 343 (1984); J. Ballam *et al.*, Phys. Rev. D **7**, 3150 (1973); W. Struczinski *et al.*, Nucl. Phys. **B108**, 45 (1976).

[29] G. Wolf, *Proceedings of the International Symposium on Electron and Photon Interactions at High Energies* (Cornell University, Ithaca, N.Y., 1971), p. 190.

[30] S. Capstick and B. D. Keister, Phys. Rev. D **46**, 84 (1992).

[31] R. Dolen, D. Horn, and C. Schmid, Phys. Rev. **166**, 1768 (1966); R. Williams, C. R. Ji, and S. Cotanch, Phys. Rev. C **46**, 1617 (1992); **43**, 452 (1991).